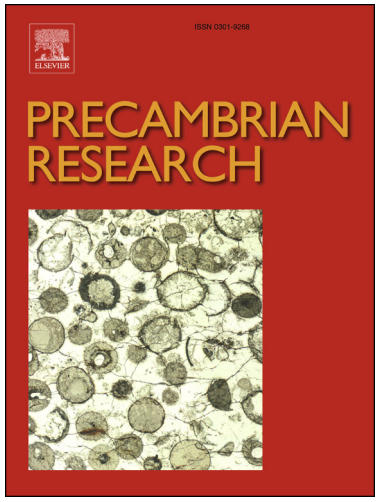
Accepted Manuscript



Long-lived metamorphic *P–T–t* evolution of the Highland Complex, Sri Lanka: insights from mafic granulites

Xiao-Fang He, Martin Hand, M. Santosh, David E. Kelsey, Laura J. Morrissey, T. Tsunogae

PII: S0301-9268(18)30084-6
DOI: https://doi.org/10.1016/j.precamres.2018.08.008
Reference: PRECAM 5155

To appear in: *Precambrian Research*

Received Date: 5 February 2018
Revised Date: 31 July 2018
Accepted Date: 20 August 2018

Please cite this article as: X-F. He, M. Hand, M. Santosh, D.E. Kelsey, L.J. Morrissey, T. Tsunogae, Long-lived metamorphic *P–T–t* evolution of the Highland Complex, Sri Lanka: insights from mafic granulites, *Precambrian Research* (2018), doi: https://doi.org/10.1016/j.precamres.2018.08.008

This is a PDF file of an unedited manuscript that has been accepted for publication. As a service to our customers we are providing this early version of the manuscript. The manuscript will undergo copyediting, typesetting, and review of the resulting proof before it is published in its final form. Please note that during the production process errors may be discovered which could affect the content, and all legal disclaimers that apply to the journal pertain.

ACCEPTED MANUSCRIPT

Long-lived metamorphic *P–T–t* evolution of the Highland Complex, Sri Lanka: insights from mafic granulites

Xiao-Fang He[1,2*], Martin Hand[2], M. Santosh[1,2,3], David E. Kelsey[2], Laura J. Morrissey[4,2], T. Tsunogae[5,6]

[1] *School of Earth Sciences and Resources, China University of Geosciences Beijing, No. 29 Xueyuan Road, Haidian District, Beijing, 100083, China*

[2] *Department of Earth Sciences, School of Physical Sciences, University of Adelaide, Adelaide, SA 5005, Australia*

[3] *State Key Laboratory of Continental Dynamics, Department of Geology, Northwest University, Xi'an 710069, China*

[4] *School of Natural and Built Environments, University of South Australia, Adelaide, Australia*

[5] *Faculty of Life and Environmental Sciences, University of Tsukuba, Ibaraki 305-8572, Japan*

[6] *Department of Geology, University of Johannesburg, Auckland Park 2006, South Africa*

**Corresponding author e-mail: geohxf@163.com; Tel.: +86-13436391699.*

ACCEPTED MANUSCRIPT

ACCEPTED MANUSCRIPT

ABSTRACT

Sri Lanka is composed of four major tectonic units known as the Wanni, Highland, Kadugannawa and Vijayan complexes, and preserves important records of the history of the Gondwana supercontinent. The Highland Complex records Neoproterozoic–Cambrian metamorphism associated with the assembly of the supercontinent Gondwana. We combine phase equilibria modelling with isotopic and trace element geochemistry to provide a time-integrated *P–T* evolution using representative garnet-bearing mafic granulites from the Highland Complex. New zircon U–Pb geochronology and garnet trace element data from one locality in the EHC, together with a dataset compiled from published results, indicate garnet and zircon existed in equilibrium during long-lived high temperature metamorphism for possibly longer than 100 Ma (ca. 660–520 Ma). Calculated pseudosections imply high-temperature to potentially ultrahigh temperature (>850 °C) conditions for peak metamorphism. The Highland Complex is characterised by a small decrease in pressure and temperature following peak conditions. This was followed by an accelerated rate of exhumation, leading to the partial replacement of garnet-bearing assemblages by lower pressure parageneses. Although the post-peak cooling/modest pressure decrease is a comparatively minor part of the *P–T* evolution, compiled zircon U–Pb data suggest it was the temporally dominant part of the thermobarometric history, comprising more than 100 Myr. The long-lived high post-peak temperatures require a stable in-situ heat source, which based on regional litho-tectonic correlations, was almost certainly elevated rates of crustal heat production. The minor cooling interval from *P–T* space is in fact is the temporally dominant part of the *P–T* evolution in the Highland Complex. This highlight that without time analysis, the *P–T* evolution does not convey the long-lived baric stability of the high-temperature history of the Highland Complex.

Keywords: U–Pb zircon geochronology; mafic granulites; calculated pseudosections; ultrahigh-temperature (UHT); phase equilibria;

1. Introduction

The Precambrian crustal basement of Sri Lanka is composed of four major tectonic units namely, the Wanni Complex (WC) and the Kadugannawa Complex (KC) to the west, the central Highland Complex (HC), and the Vijayan Complex (VC) to the east (Fig. 1). The Highland Complex (HC) records widespread Late Neoproterozoic–Cambrian granulite-facies metamorphism, including evidence for ultrahigh temperature (UHT) metamorphism (Dharmapriya et al., 2015b and refernces therein).

Numerous detailed petrological studies on metapelitic UHT granulites have been carried out in this terrane (Hapuarachchi, 1968; Katz, 1971, 1972; Sandiford et al., 1988; Burton and

ACCEPTED MANUSCRIPT

O'Nions, 1990; Schenk et al., 1991; Faulhaber and Raith, 1991; Osanai et al., 2000, 2006, Sajeev and Osanai, 2004b, 2004a, 2005, Dharmapriya et al., 2014, 2015a, 2015b). The calculated pressure–temperature (*P–T*) estimates from these studies have concentrated on metasedimentary rocks, for which a large number of conventional thermobarometers exist. Conventional thermobarometry estimates may be based on a variety of different thermometers and barometers which use different thermodynamic and activity–composition relations, and it requires assumptions as to which parts of the minerals used are in equilibrium. Therefore, it is difficult to test the reliability of the *P–T* estimates as well as to correlate *P–T* conditions from different studies (e.g. Morrissey et al., 2017). The release of new activity–composition models for high temperature amphibole, clinopyroxene and tonalitic melt in mafic systems (Green et al., 2016) allow us to revisit the existing *P–T* estimates from the mafic granulites of the HC.

Previous studies on the HC domain interpreted it to be part of a supracrustal basin developed in a suture zone with the Lützow–Holm Complex in East Antarctica during the final phase of Gondwana assembly (Takahashi et al., 2018; Takamura et al., 2018). The WC, KC and VC domains are considered as Grenvillian-aged terranes formed in arc-related settings at the outer margin of the Rodinia supercontinent (Kehelpannala, 2003, 2004, Kröner et al., 2003, 2013; Willbold et al., 2004) or as an island arc terrane (Archibald et al., 2017). In a more recent study by Santosh et al. (2014), a double-sided subduction model is presented where the WC and the VC represent continental arcs on opposite sides of a Neoproterozoic ocean, culminating in collision along the HC during the late Neoproterozoic–Cambrian. The different interpretations for the tectonic models suggest it is necessary to re-evaluate the possible tectonic scenarios.

In this study, we utilise the new activity–composition models that allow investigation of metabasic rocks to constrain the *P–T* record of mafic granulites from both eastern and western margins of the Highland Complex, Sri Lanka. New laser ablation–inductively coupled plasma–mass spectrometry (LA–ICP–MS) zircon age data are reported and combined with garnet/zircon rare earth element (REE) data to better constrain the duration of high temperature metamorphism. Our integrated results show that variation between zircon ages in each location is likely to be the result of a single, prolonged UHT metamorphic event. These data are integrated to evaluate the tectonic setting of the Sri Lankan components of Gondwana.

2. Geological background

2.1. Sri Lanka and the Highland Complex

The metamorphic basement of Sri Lanka is subdivided into three major approximately north–south trending complexes based on stratigraphic correlation and metamorphic grade (Kröner et al., 1991; Cooray, 1994). These are the Vijayan Complex (VC) in the east consisting of

ACCEPTED MANUSCRIPT

amphibolite facies rocks, the Highland Complex (HC) in the centre consisting of granulite facies rocks, and the Wanni Complex (WC) in the west composed of upper amphibolite to granulite facies metasediments and meta-igneous rocks (Fig. 1a). Later research identified the area towards the northwestern part of Kandy as the distinct Kadugannawa Complex (KC), which forms doubly-plunging synforms containing rocks metamorphosed at upper amphibolite to granulite facies conditions and is interpreted to represent a Neoproterozoic disrupted arc magma chamber (Milisenda et al., 1988; Kröner et al., 1991; Cooray, 1994).

The dominant lithologies in the HC are metasedimentary rocks (quartzite, marble, calc-silicate, and metapelite) and meta-igneous rocks (charnockite and mafic granulite) (Kröner et al., 1994; Kröner et al., 1994; Kröner and Jaeckel, 1994; Braun and Kriegsman, 2003; Santosh et al., 2014; Takamura et al., 2015). Rocks of the HC were metamorphosed to regional granulite-facies conditions (Perera, 1984; Faulhaber and Raith, 1991; Hiroi et al., 1994; Raase and Schenk, 1994; Schumacher and Faulhaber, 1994). Evidence for UHT metamorphism has been reported at several localities from pelitic, mafic and quartzo-feldspathic granulites in the central HC (Kriegsman and Schumacher, 1999; Osanai et al., 2000, 2006, Sajeev et al., 2003, 2007, 2010; Sajeev and Osanai, 2004a; Dharmapriya et al., 2015b; Malaviarachchi and Dharmapriya, 2015) and rarely from the southwestern part (Sajeev and Osanai, 2004b). The pelitic UHT granulites of Sri Lanka are commonly interlayered with psammitic to semipelitic metasediments or charnockitic rocks (Osanai et al., 2006). In outcrop, metasedimentary rocks of the HC are usually migmatitic and have a gneissic texture. Leucosomes are typically concordant, but discordant leucosomes are not uncommon, suggesting that anatectic melts were present over a long time interval during the high-grade deformation history (Raase and Schenk, 1994).

Estimated conditions from both metasedimentary and metabasic rocks in the western HC range from pressures of less than 8 kbar to in excess of 15 kbar and temperatures of less than 800 to over 1200 °C (Fig. 2). However, the metamorphic conditions are poorly constrained for the eastern HC. Two contrasting *P–T–time* (t) paths, one for metasedimentary rocks and the other for meta-igneous rocks, were interpreted for the HC rocks in previous studies (Fig. 2). A clockwise *P–T–t* path was inferred for the metasedimentary rocks on the basis of: (1) rare early kyanite and staurolite; (2) abundant peak sillimanite; (3) breakdown of garnet to cordierite-bearing assemblages; and (4) late andalusite (Perera, 1984; Sandiford et al., 1988; Hiroi et al., 1994; Ellis and Hiroi, 1997). The clockwise *P–T* path suggested by Raase and Schenk (1994) and Kriegsman and Schumacher (1999) consists of a near-isobaric prograde heating segment followed by a near-isothermal down-pressure retrograde segment. In contrast, a near-isobaric cooling path followed by a pressure and temperature decrease after peak metamorphism was inferred for meta-igneous rocks based on garnet coronas around orthopyroxene and plagioclase (Schumacher et al., 1990; Prame, 1991; Schenk et al., 1991).

ACCEPTED MANUSCRIPT

Compared to those in the western Highland Complex (WHC), the UHT granulites in the eastern Highland Complex (EHC) are less studied. Osanai et al. (2006) reported aluminous corundum–garnet–sillimanite–spinel–quartz gneiss in the eastern central Highland Complex and inferred a multi-stage clockwise retrograde *P–T* path using petrogenetic grids, but peak *P–T* conditions were unconstrained. Mathavan and Fernando (2001) reported calc-silicate granulites from Buttala Klippe at the eastern margin of the EHC and suggested peak metamorphic conditions of 875–900 °C and 9 kbar and inferred high-temperature isobaric cooling to < 675 °C. Fernando et al. (2003) obtained peak metamorphic conditions of ~ 875 °C and 9 kbar from mafic granulite through two-pyroxene thermometry and garnet–clinopyroxene–plagioclase–quartz barometry, and inferred a slow cooling history due to the nearly identical composition of garnet rims and cores.

2.2. Mafic granulite in the Highland Complex

The *P–T* conditions and the metamorphic evolution of the mafic granulites from the western Highland Complex (WHC) have been studied by some workers using thermobarometry (Kriegsman and Schumacher, 1999; Fernando et al., 2003; Osanai et al., 2006; Sajeev et al., 2007; Santosh et al., 2014; Takamura et al., 2015). Sajeev et al. (2007) studied garnet–clinopyroxene–orthopyroxene granulites that are exposed mainly in Victoria Dam towards the southeastern part of Kandy (Fig. 2a). These rocks occur as lenses or blocks within layered pelitic granulites and calc-silicate rocks. They are relatively coarse-grained, weakly foliated and consist mainly of garnet, orthopyroxene, clinopyroxene, plagioclase and amphibole with subordinate quartz, magnetite, apatite and zircon. Most garnet porphyroblasts are surrounded by orthopyroxene–plagioclase symplectites. Sajeev et al. (2007) reported a peak temperature of ~ 925 °C at a minimum peak pressure of 12.5 kbar from calculated garnet–clinopyroxene thermobarometry and petrogenetic grids. Conventional thermobarometry results by Takamura et al. (2015) using the garnet–clinopyroxene thermometer yielded temperatures of 810–850 °C, and the garnet–clinopyroxene–plagioclase–quartz barometer gave pressures of 8.5–9.0 kbar. They also obtained a U–Pb zircon age of ca. 580 Ma for the mafic granulite, interpreted as the timing of peak metamorphism. Santosh et al. (2014) reported two groups of ages, at 576.8 ± 9.3 Ma and 523.0 ± 7.1 Ma, from garnet-bearing metagabbro in the HC, suggesting two distinct thermal events.

Mafic granulites are less studied in the EHC (Schenk et al., 1991; Schumacher and Faulhaber, 1994; Takamura et al., 2015; Osanai et al., 2016a, 2016b). Osanai et al. (2016a) reported coarse-grained, homogeneous and weakly foliated mafic granulite with a garnet–orthopyroxene–plagioclase peak assemblage. Quartz typically occurs as inclusions in garnet. They obtained U–Pb zircon ages of 636–517 Ma for the mafic granulite and interpreted that it was formed by multiple thermal episodes at ca. 620–580 and 563–525 Ma. Due to an overall

ACCEPTED MANUSCRIPT

lack of reaction microstructures in this area, the authors did not study the metamorphic evolution of the mafic granulites.

The previous studies show that mafic granulites from the WHC consistently show development of extensive orthopyroxene–plagioclase symplectite microstructures surrounding garnet (Osanai et al., 2006; Sajeev et al., 2007; Santosh et al., 2014; Takamura et al., 2015), whereas those from the EHC rarely display such microstructures (Fernando et al., 2003, Osanai et al., 2016a). These different reaction textures have been used to suggest a different retrograde evolution for the EHC and WHC (Osanai et al., 2006; Sajeev et al., 2007; Santosh et al., 2014; Takamura et al., 2015). However, due to the disparate approaches, there is no direct comparison between these two regions, leading to confusion about the regional significance of the *P–T* conditions and *P–T* paths, and consequently disagreement about the tectonic evolution.

3. Analytical methods

3.1. Petrography and mineral chemistry

The locations of the samples analysed in this study are given in Supplementary Data Table S1 and plotted in Fig. 1b. Polished thin sections for petrographic studies were prepared from representative samples at the School of Earth and Space Sciences, Peking University. Electron microprobe analyses and backscattered electron (BSE) imaging were carried out using an electron microprobe analyser (JEOL JXA8530F) at the Chemical Analysis Division of the Research Facility Centre for Science and Technology, the University of Tsukuba, Japan. The analyses were performed using a 15 kV accelerating voltage and 10 nA probe current, and the data were regressed using an oxide-ZAF correction program supplied by JEOL. Representative compositions of minerals are given in Supplementary Data Table S2.

3.2. LA–ICP–MS zircon U–Pb geochronology and trace elements analysis

Zircon separation involved gravimetric and magnetic techniques from one crushed rock, sample VC-HC-8/1 from the EHC, followed by hand picking under a binocular microscope at the Yu'neng Geological and Mineral Separation Survey Centre, Langfang city, Hebei Province, China. Individual grains were mounted onto double-sided adhesive tape and enclosed in epoxy resin discs. The discs were polished to expose zircon centres and gold coated for CL imaging and U–Pb isotope analysis. Zircons were imaged under both transmitted and reflected light, and were imaged using cathodoluminescence (CL) to study the morphology and internal structures, and to choose target sites for U–Pb analyses. The CL imaging at the Beijing Geoanalysis Centre used a scanning electron microscope (JSM510) equipped with Gatan CL detector.

ACCEPTED MANUSCRIPT

U–Pb dating and trace element analysis of zircon were simultaneously conducted by laser ablation–inductively coupled plasma–mass spectrometry (LA–ICP–MS) at the Key Laboratory of Continental Collision and Plateau Uplift, Institute of Tibetan Plateau Research, Chinese Academy of Science, Beijing, China. Laser sampling was performed using a GeolasPro laser ablation system that consists of a New Wave Research UP193FX excimer laser (wavelength of 193 nm and maximum energy of 200 mJ) and a homogenizing imaging optical system. An Agilent 7500a ICP–MS instrument was used to acquire ion-signal intensities. The ablated samples were then transported from laser to ICP–MS by helium carrier gas through a 3-mm diameter PVC tube and mixed with high-purity argon gas just before entering the ICP–MS torch. This reduces elemental fractionation of the sample. A spot size of 35 μm with a repetition rate of 8 Hz and spot energy density of 8–10 J/cm^2 was used for ablation. This produced 15 to 20 μm-deep pits within the zircon. A single grain analysis time was 100 s (15 s with laser off, 40 s with laser on, 45 s of delays including background measurement). Raw count rates for ^{29}Si, ^{49}Ti, ^{89}Y, ^{90}Zr, ^{93}Nb, ^{139}La, ^{140}Ce, ^{141}Pr, ^{146}Nd, ^{147}Sm, ^{153}Eu, ^{157}Gd, ^{159}Tb, ^{163}Dy, ^{165}Ho, ^{166}Er, ^{169}Tm, ^{172}Yb, ^{175}Lu, ^{179}Hf, ^{181}Ta, ^{202}Hg, ^{207}Pb, ^{206}Pb, ^{208}Pb, ^{232}Th, and ^{238}U were collected. Three dwell times were used: 30 μs for all four Pb isotopes, 6 μs for ^{29}Si, ^{90}Zr, 15 μs for ^{232}Th, ^{238}U and 10 μs for the remaining isotopes.

Plešovice zircon and NIST610 glass were used as external standards for U–Pb dating and trace element calibration, respectively. Time-dependent drifts of U–Th–Pb isotopic ratios were corrected using a linear interpolation (with time) for every ten analyses. Analyses of the primary standard Plešovice throughout the study yielded a weighted mean ^{206}Pb/^{238}U age of 337.1 ± 3.2 Ma (n = 20, MSWD = 0.02). Zircon standard 91500 was treated as an unknown to monitor the stability and accuracy of acquired U–Pb data. The weighted mean ^{206}Pb/^{238}U age for secondary standard 91500 in this study is 1090 ± 10 Ma, n = 10, MSWD = 0.68, which is outside uncertainty of the published value of 1061 ± 4 Ma (Jackson et al., 2004). Validation results from 91500 (without propagation for systematic uncertainties) highlighted the need for an additional variance component (2.5% 2σ). Propagating this systematic uncertainty into the individual uncertainty of the sample result follows Horstwood et al. (2016). Trace element composition of zircon was calibrated with ^{29}Si as internal standard.

GLITTER 4.0 software (Griffin et al., 2004) was used to perform off-line data reduction and integration of background and ablation signals. Time-drift correction and quantitative calibration was applied for trace element analysis and U–Pb dating. Final assessment of uncertainty and data visualization were done in Excel™ using Isoplot/Ex_ver4.15 (Ludwig, 2012). Errors are quoted at the 2σ level. Full isotopic data can be found in Supplementary Data Table S3.

ACCEPTED MANUSCRIPT

3.3. LA–ICP–MS *in-situ* garnet trace element analysis

Trace element analyses of garnet grains from the EHC sample VC-HC-8/1 were done at Adelaide Microscopy, the University of Adelaide, with an ASI Resolution ArF Excimer laser ablation system with a S150 large format sample chamber. The laser was coupled to an Agilent 7900x ICP–MS. Samples were ablated with a spot size of 43 µm with an energy at the sample surface of ~3.5 J/cm^2 and a repetition rate of 5 Hz. Samples were ablated in a He atmosphere (flow rate 0.35 L/min) and the aerosol mixed with Ar carrier gas (flow rate 1.01 L/min) for transport to the ICP–MS. In-house standard NIST612 was used as the primary standard for calibration and drift correction, and GSD-1G was used as a secondary standard. The total acquisition time of each analysis was 90 s. This included 30 s of background measurement, one cleaning pulse and 60 s of sample ablation. The following elements were measured: ^{23}Na, ^{24}Mg, ^{27}Al, ^{29}Si, ^{43}Ca, ^{57}Fe, ^{89}Y, ^{139}La, ^{140}Ce, ^{141}Pr, ^{146}Nd, ^{147}Sm, ^{153}Eu, ^{157}Gd, ^{159}Tb, ^{163}Dy, ^{165}Ho, ^{166}Er, ^{169}Tm, ^{172}Yb, ^{175}Lu, with counting times of 0.005–0.060 seconds for each mass and a total sweep time of 0.26 seconds. Data was processed using Iolite software (Paton et al., 2011) using ^{43}Ca as an internal standard and concentrations in reference materials GSD-1G and NIST612 from Guillong et al., (2005) and Jochum et al., (2011). Full isotopic data can be found in Supplementary Data Table S4.

3.4. Phase equilibria modelling

P–T pseudosections were calculated for three samples of mafic granulite from the EHC. *P–T* pseudosections were also calculated for two samples of mafic granulite from the WHC for comparison, based on bulk chemistry data from Takamura et al. (2015).

Samples VC-HC-8/1, -8/2, and -8/3 do not preserve mineral reaction microstructures. Therefore, chemical compositions for phase equilibria modelling were determined by whole-rock geochemical analysis of rocks that are devoid of surface alteration or weathering. The samples were reduced in a jaw crusher and then manually fine-powdered in an agate mortar. Whole-rock major-oxides and trace-elements including rare earth elements (REE) were analysed by XRF instruments at the National Research Centre of Geoanalyses, Beijing (China).

The principal uncertainties in the bulk composition for calculating phase equilibria relate to Fe_2O_3 and H_2O (Johnson and White, 2011). For samples VC-HC-8/1, -8/2 and -8/3, wet chemistry methods were used to determine the amount of FeO and Fe_2O_3. The H_2O^+ value from whole-rock geochemical analysis was used to determine the H_2O contents for samples VC-HC-8/1, -8/2 and -8/3. Combined (lattice) water content was determined with the equation H_2O^+ % = $(m_2–m_3)/(m_2–m_0)$ ×100, $(m_2–m_0)$ = weight of sample dried at 105 °C, $(m_2–m_3)$ =

ACCEPTED MANUSCRIPT

weight of water after heating dried sample to a very high temperature (over 1000 °C). The whole-rock compositions are presented in Supplementary Data Table S5.

Samples HC8 and HC7 are mafic granulites from the EHC reported by Santosh et al. (2014) and Takamura et al. (2015). Bulk compositions for modelling were taken from Takamura et al. (2015) with the modification that Fe^{2+}/Fe^{3+} ratios were derived from the calculated ferric iron content of the mineral analyses reported by Takamura et al. (2015) following Droop (1987). This modification was necessary because the FeO content reported by Takamura et al (2015) was not reconcilable with the reported Fe_2O_3 content.

Phase equilibria calculations were performed using the software program THERMOCALC v3.40 (Powell and Holland, 1988; Holland and Powell, 2011) in the model chemical system MnNCKFMASHTO ($MnO–Na_2O–CaO–K_2O–FeO–MgO–Al_2O_3–SiO_2–H_2O–TiO_2–O$), where 'O' is a proxy for Fe_2O_3, using the latest internally-consistent thermodynamic dataset 'ds6' (filename tc-ds63.txt; Holland and Powell, 2011) and activity–composition models (Green et al., 2016). Contours of phase modes and compositions were calculated and plotted using TCInvestigator software (Pearce et al., 2015). The observed mineral vol.% abundances were determined by pixel counting of scanned thin sections photos in Adobe Photoshop then converted to mole percent using molar volume data from Holland and Powell (2011), thus allowing for direct comparison with THERMOCALC output (Supplementary Data Table S1).

4. Results

4.1. Samples and petrography

This study uses a combination of three samples (VC-HC-8/1, -8/2 and -8/3) that were sampled from the EHC by authors in this study, and two samples (HC8 and HC7) from the WHC that were studied by Takamura et al. (2015) (Fig. 1).

VC-HC-8/1: EHC

Samples VC-HC-8/1, -8/2, and -8/3 were collected from a road cutting along the Beragala–Haputale Road near Haputale (Supplementary Data Table S1). The mafic granulites occur as massive lenses/blocks within banded charnockite (Fig. 3a). The rock is mostly homogeneous without an obvious foliation or deformation (Fig. 3b), but no massive magmatic structure is observed from the outcrop. In places, localized small domains of the rock are locally more felsic (Fig. 3c). Sample VC-HC-8/1 is composed of garnet, clinopyroxene, orthopyroxene, hornblende, plagioclase and ilmenite (Fig. 4a, b). Medium- to coarse-grained (1.0–3.0 mm) garnet is porphyroblastic (Figs. 3d and 4a) and contains numerous inclusions of clinopyroxene, orthopyroxene, apatite, plagioclase, ilmenite, quartz and hornblende (Fig. 4a). Medium to

ACCEPTED MANUSCRIPT

coarse-grained (0.5–2.5 mm) and subidioblastic clinopyroxene is the dominant matrix mineral and occurs as aggregates, together with fine-grained orthopyroxene and ilmenite. Xenoblastic plagioclase is medium- to coarse-grained (0.5–1.5 mm) and forms the matrix together with garnet and pyroxenes. Hornblende is medium- to coarse grained (0.5–1.5 mm) and occurs along grain boundaries between garnet and pyroxene (Fig. 4b). Aggregates of subidioblastic and medium- to coarse-grained (0.5–1.5 mm) hornblende define amphibole-rich domains of the rock (Fig. 4a, b). Fine- to medium-grained (0.3–1.0 mm), rounded ilmenite grains occur commonly either in the matrix or as inclusions in garnet. Image analysis software shows the following: (1) garnet comprises 20 vol.% of the sample and predominantly occurs within plagioclase-rich domains; (2) clinopyroxene comprises 28 vol.% of the sample with the remainder comprising plagioclase, orthopyroxene, hornblende and oxides.

VC-HC-8/2: EHC

Sample VC-HC-8/2 shows similar character to sample VC-HC-8/1 but with slightly different mineral abundances. It is composed of garnet, clinopyroxene, plagioclase, hornblende, orthopyroxene and ilmenite, with accessory zircon (Fig. 4d). Needle-like rutile is widely present as probable exsolution lamellae in orthopyroxene (Fig. 4d). Image analysis shows similar mineral abundance as sample VC-HC-8/1 (garnet 21 vol.%, clinopyroxene 28 vol.%).

VC-HC-8/3: EHC

Sample VC-HC-8/3 was collected from a garnet-rich part of the outcrop and is composed of garnet, clinopyroxene, hornblende, plagioclase, orthopyroxene, and ilmenite. Hornblende, clinopyroxene and orthopyroxene occur as aggregates in the matrix around garnet porphyroblasts (Fig. 4e), some of the hornblende is replaced by garnet, orthopyroxene and plagioclase (Fig. 4f). Image analysis shows (1) garnet comprises 24 vol.% of the sample and predominantly occurs within hornblende-rich domains; (2) clinopyroxene comprises 25 vol.% of the sample, with the remainder comprising plagioclase, orthopyroxene, hornblende and oxides.

HC7: WHC

Samples HC8 and HC7 are mafic granulites studied by Takamura et al. (2015). Sample HC7 was collected from a road-side outcrop along the Kandy–Hantana Road near Deiyannewela (Fig. 1c). The rock occurs as lenses a few meters in length within foliated quartzite and psammitic–pelitic gneisses. In hand specimen, sample HC7 is a medium- to coarse-grained and massive mafic granulite without any obvious foliation or lineation (Fig. 3b in Takamura et al. 2015). The description of Takamura et al. (2015) does not permit an evaluation of whether melt was present. The rock is composed of garnet, clinopyroxene, plagioclase, orthopyroxene,

ACCEPTED MANUSCRIPT

ilmenite, and hornblende (Fig. 4a, b in Takamura et al., 2015). Quartz and biotite occur as inclusions in garnet. Takamura et al. (2015) and Santosh et al (2014) present close-up field photographs (Fig. 3d in Takamura et al., 2015; Fig. 4c in Santosh et al., 2014) of fresh 14 by 9 cm outcrop of TC7. Using these figures, image analysis software shows that garnet comprises between 3–12 vol.% of the rock. However, photomicrographs presented by Takamura et al (2015) and Santosh et al (2014) contain 18 vol.% and 35 vol.% garnet respectively. Therefore, it seems likely the photomicrographs over represent the volume of garnet with respect to the outcrop. We prefer to base on the volume proportions on the visual evidence they provide of the outcrop.

HC8: WHC

Sample HC8 (Fig. 1c) was collected from the Hantana area, approximately 1.8 km south from the locality of HC7. This rock is also medium- to coarse-grained and massive with no obvious foliation or lineation and occurs as blocks in quartzite, although the contact between the two lithologies is obscured (Fig. 3c in Takamura et al. 2015). The rock contains patches of coarse-grained orthopyroxene and garnet surrounded by comparatively felsic patches, typical of residual peritectic phases after melt loss. This rock is composed of garnet, clinopyroxene, plagioclase, orthopyroxene, quartz, ilmenite, and hornblende with accessory rutile, titanite, biotite, and zircon (Fig. 4c, d in Takamura et al. 2015; Fig. 5i in Santosh et al 2014). Image analysis of a fresh outcrop photograph (Fig. 3d in Takamura et al. 2015) indicates that it contains 30 vol.% garnet, 23 vol.% plagioclase and 47 vol.% combined pyroxenes, amphibole and oxides. It also contains mineral reaction microstructures that are characterised by symplectites and/or domains of orthopyroxene and plagioclase surrounding garnet and separating it from quartz and clinopyroxene. Hornblende sporadically occurs along garnet boundaries.

4.2. Mineral chemistry

Electron microprobe data was collected from sample VC-HC8/1. Representative electron microprobe compositions of minerals including garnet, pyroxene, amphibole, plagioclase and ilmenite are provided in Supplementary Data Table S2.

Garnet in sample VC-HC-8/1 is mostly almandine-rich with no significant core–rim variation. Garnet has consistent X_{Fe} (= Fe/(Mg+Fe)) of around 0.63, with almandine proportion (X_{alm}) of 0.50–0.51, pyrope (X_{py}) proportion of 0.29, grossular proportion (X_{grs}) of ~0.17 and minor spessartine proportion (X_{sps}) of 0.024–0.025.

Clinopyroxene in sample VC-HC-8/1 is Mg-rich and compositionally unzoned. X_{Fe} is in the range 0.27–0.29. Clinopyroxene from the matrix has a similar composition to clinopyroxene

ACCEPTED MANUSCRIPT

included in garnet. Orthopyroxene grains are also homogeneous and Mg-rich with X_{Fe} values of 0.38–0.39 and Al contents of 0.19–0.20 p.f.u.

Amphibole in sample VC-HC-8/1 is characterized by high Ca (Ca > 1.8 p.f.u) and high alkali content (Na+K >0.9 p.f.u). It shows slight compositional variation depending on microstructural location. It is calcic amphibole–pargasite in composition (Leake et al., 1997). Amphibole inclusions in garnet have lower X_{Fe} values (0.31–0.32) than amphibole occurring in the matrix (0.39–0.42). There is no compositional variation between matrix amphibole grains near garnet and those grains near clinopyroxene.

Plagioclase in sample VC-HC-8/1 is anorthite-rich (An_{49-52}) and shows no compositional variation from core to rim. Plagioclase inclusions in garnet have slightly higher An content than those in the matrix.

4.3. Zircon U–Pb geochronology

Zircon grains from sample VC-HC-8/1 range in length from 50–200 μm, are mostly rounded in shape and have length to width ratios of 1:1. Most are light brown to dark brown and transparent to translucent. The CL images show relatively homogeneous textures, although some grains show weak patchy zoning and core–rim texture (Fig. 5). Most zircon grains display a narrow (<10 μm) rim with low CL response.

A total of 28 spots were analysed from 28 zircon grains (Fig. 5). Th contents range from 1 to 107 ppm and U contents range from 1 to 285 ppm, with Th/U ratios in the range 0.02–0.67 (Supplementary Data Table S3). Notably, the lowest Th/U ratios are from older zircon grains, with an increase in the Th/U ratios to younger ages (Fig. 6a, b). Four grains (spots 10, 13, 19, 20) that are highly (>15 %) discordant were excluded. The remaining 24 analyses plot on or near the concordia line on a Tera-Wasserburg inverse concordia diagram (Fig. 6a). The two oldest grains (spots 1, 11) yield $^{206}Pb/^{238}U$ ages of 1219 ± 16/34 Ma and 794 ± 10/22 Ma (without/with propagation for systematic error), and are interpreted to be inherited. The three youngest analyses (spots 3, 27, 28) form a coherent group with a weighted average $^{206}Pb/^{238}U$ age of 522 ± 14/19 Ma (n = 3, MSWD = 1.5). The remaining 19 analyses yield $^{206}Pb/^{238}U$ ages varying from 666 to 567 Ma.

4.4. Zircon and Garnet LA–ICP–MS trace elements

4.4.1. Zircon

Zircon REE compositions for sample VC-HC-8/1 display variable concentrations whereas garnet shows a much more homogeneous composition. The general distribution patterns show enrichment in HREE compared to LREE (Fig. 7c). Average Gd_N (subscript N denotes chondrite normalisation after Sun and McDonough, 1989) values are 1.5–71.0. Yb_N values are 30–1559 with a distinct positive slope to the middle-heavy REE profile. Yb_N/Gd_N ratios range

ACCEPTED MANUSCRIPT

from 5–68. All analyses except the two oldest grains show no significant Eu anomalies with Eu/Eu* values of 0.53–1.18 (Supplementary Data Table S4). The two old, inherited zircons grains have the highest total REE, obvious negative Eu anomalies (Eu/Eu* values of 0.13–0.60), Gd_N values of 63–71 and Yb_N of 1515–1559, giving Yb_N/Gd_N values of 21–25. Zircon age vs. Yb_N and zircon age vs. Yb_N/Gd_N plots (Supplementary Fig. S1) do not show characteristic relationships.

4.4.2. Garnet

Garnet from sample VC-HC-8/1 shows limited or no core to rim variation (Fig. 7d). Gd_N values in all analysed garnet grains are 17.7–28.0 with an average of 25, Yb_N values are 26.2–116.9 with a negative slope to the heavy REE profile, Yb_N/Gd_N values are 1.0–4.8 and Yb_N/Dy_N are 0.6–1.9. All garnet analyses show little or no negative Eu anomalies with Eu/ Eu* values of 0.8–1.0 (Supplementary Data Table S6). Y values range from 58.4 to 122.3, with similar variation in core and rim analyses (64.3–114.3 and 58.4–122.3, respectively).

D_{REE} zircon/garnet values for sample VC-HC-8/1 from this study show varied patterns between the magmatic and metamorphic zircon and garnet associated with different age groups (Rubatto and Hermann, 2007; Taylor et al., 2015, 2017), which suggesting different zircon and garnet growth relationships. Analysed inherited magmatic zircon cores show *D* values that strongly favour zircon for the HREE (steep D_{REE} profiles) (Fig. 7a) and therefore are unlikely to reflect growth during metamorphism. Strictly speaking, D values should not be calculated for phases that grow at different times, but here we use the values to differentiate zircon age groups. D_{REE} (zircon/garnet) partition coefficients close to unity strongly suggest that the metamorphic ages from this study reflect zircon growth in the presence of garnet (Taylor et al., 2015b, 2017). Although the results in the D_{REE} (zircon/garnet) array plot are more scattered than in Fig. 7a. The 660–560 Ma zircon analyses show low log (D_{Yb} (Zrn/Grt)/ D_{Gd} (Zrn/Grt)) and log (D_{Yb} (Zrn/Grt)), plotted at high T area, while the youngest group (ca. 520 Ma) of zircon plot at low T range according to the new array plot modelled by Taylor et al. (2017).

4.5 Phase equilibria modelling

4.5.1. Samples VC-HC-8/1, 8/2 and 8/3 from EHC

The interpreted peak mineral assemblage in sample VC-HC-8/1 is garnet–clinopyroxene–orthopyroxene–plagioclase–hornblende–ilmenite (Fig. 8a). The rocks do not have a migmatised texture. The presence of orthopyroxene provides an upper pressure constraint, whereas the absence of olivine provides a lower pressure constraint. The peak assemblage occurs down temperature of the solidus between ~ 850–980 ºC at pressures between 7.0 and 10.3 kbar (Fig. 8a).

ACCEPTED MANUSCRIPT

Sample VC-HC-8/2 has a very similar composition to VC-HC-8/1, but the slightly lower H_2O content results in a slightly higher temperature solidus. The interpreted peak assemblage is hornblende + clinopyroxene + orthopyroxene + garnet + plagioclase + ilmenite. The peak assemblage occurs at very similar conditions to VC-HC-8/1 (Fig. 8b).

Sample VC-HC-8/3 has 0.2–0.4 mol.% more H_2O than the other two samples, resulting in a lower temperature solidus and increased biotite stability to higher temperature (Fig. 8c). The peak assemblage in sample VC-HC-8/3 is the same as in the previous samples. The peak assemblage occurs at *P–T* conditions of 6.5–10 kbar and 870–950 ºC (Fig. 8c).

The modal proportion of garnet in these samples provides some additional pressure constraints. Garnet abundance is 22 and 23 mol.% (20 and 21 vol.%) in samples VC-HC-8/1 and -8/2 and 27 mol.% (24 vol.%) in -8/3. The garnet modes from all three samples refine the peak pressures to be 8–9 kbar.

4.5.2. Samples HC8 and HC7 from WHC

Sample HC8 contains garnet–plagioclase–orthopyroxene–clinopyroxene–rutile–quartz–ilmenite–hornblende (Takamura et al., 2015), and the rock is not migmatitic, suggesting the *P–T* conditions were subsolidus. Takamura et al. (2015) interpreted the peak assemblage to have been garnet–plagioclase–orthopyroxene–clinopyroxene–rutile–quartz. However, this assemblage is not stable at subsolidus conditions (Fig. 8d). Instead modelled subsolidus assemblages are calculated to contain biotite and hornblende. However, the mole percent of biotite calculated with THERMOCALC is very low (<1.5 mol.%). Such low abundance of biotite would be difficult to observe visually or another possibility is that the prediction of biotite in the pseudosections is related to the uncertainties in the thermodynamics of biotite models which makes that biotite appears as a stable phase in the calculations. Therefore, we suggest the perceived (visual) peak assemblage was garnet–plagioclase–orthopyroxene–clinopyroxene–rutile–quartz–hornblende. In addition, the photomicrographs presented by Takamura et al. (2015) contain coarse ilmenite, suggesting garnet–plagioclase–orthopyroxene–clinopyroxene–rutile–quartz–ilmenite–hornblende was stable or the rock evolved from a rutile-bearing assemblage to an ilmenite-bearing assemblage. Fig. 8d shows there is a narrow *P–T* field that contains garnet-plagioclase–orthopyroxene–clinopyroxene–rutile–quartz–ilmenite–hornblende. Image analysis of the outcrop sampled by Takamura et al. (2015) indicates the rock has 30 vol.% (33 mol.%) garnet, consistent with the modelled volumes of garnet in the *P–T* pseudosection. However, the mineral equilibria model does not provide a lower estimate on temperature as the fields are open to lower temperature within the modelled *P–T* range.Garnet–clinopyroxene thermometry using activity composition models from Holland & Powell (1998) and Powell & Holland (1999) and the mineral compositions reported by Takamura et al. (2015) give a temperature range of 815–835 ºC in subsolidus fields that

ACCEPTED MANUSCRIPT

contain garnet–plagioclase–orthopyroxene–clinopyroxene–quartz ± ilmenite, rutile. This temperature range is just below the modelled solidus. The temperature estimate from thermobarometry and the garnet modes suggest sample HC8 records conditions of 840 ºC and 9.2 kbar. The presence of orthopyroxene–plagioclase symplectites implies that rock records a decrease in pressure. However the abundance of garnet and comparative paucity of symplectite suggests that this rock records a limited pressure decrease.

Sample HC7 contains the assemblage garnet–plagioclase–orthopyroxene–clinopyroxene–ilmenite. This assemblage occupies a wide range of *P–T* space that is unbounded to lower temperatures within the modelled *P–T* domain. The garnet mode in HC7 is average ~8 vol.% (~9 mol.%), with garnet commonly located within patches of plagioclase within an orthopyroxene-bearing matrix, consistent with reaction progress to remove garnet. The low garnet mode suggests the recorded *P–T* conditions lie close to the lower pressure boundary of the garnet–plagioclase–orthopyroxene–clinopyroxene–ilmenite field, which constrains pressures to between ~ 4.5 and 5.5 kbar. A potential temperature constraint can be derived from garnet–clinopyroxene thermometry using mineral compositions reported by Takamura et al. (2015), which gives temperatures in the range 770–790 ºC between 4.5 and 5.5kbar.

5. Discussion

5.1. Metamorphic evolution of the mafic granulites

5.1.1. Peak and retrograde evolution

The calculated *P–T* pseudosections for the peak and retrograde metamorphic conditions are presented in Fig. 8. For the samples from the EHC, the recorded *P–T* conditions appear to be around 900 ºC and 8–9 kbar. These samples show no retrograde reaction microstructures, in particular no symplectites or coronas around garnet that have been reported from the Highland Complex by a number of authors (Schenk et al., 1991; Schumacher and Faulhaber, 1994). The lack of retrograde reaction microstructures indicates either that the samples were unreactive, or evolved in *P–T* space along contours of constant mode, which for these samples are modelled to have gentle positive slopes. This means the samples could have evolved down pressure and temperature without reaction microstructure development.

In contrast to the samples from the EHC, the samples from the WHC described by Takamura et al. (2015) and remodelled in this paper show more thermobarometric diversity. Sample HC8 contains abundant garnet, and although it contains orthopyroxene–plagioclase symplectites that fringe garnet, the abundance of garnet means the sample records pressures similar to those inferred for VC-HC-8/1-3. Therefore the reaction microstructures indicate the sample

ACCEPTED MANUSCRIPT

records some decrease in pressure. However Takamura et al. (2015) provided no information on the modal abundance of the reaction textures, and therefore it is difficult to constrain the maximum pressure the peak assemblage formed at. Takamura et al. (2015) describe ilmenite inclusions in garnet and clinopyroxene, as well as ilmenite being a matrix mineral. They additionally describe rutile as an accessory mineral that occurs in the matrix. These relationships suggest rutile formed comparatively late and after ilmenite-bearing assemblages. In this case, it is likely the sample reached pressures not significantly greater than recorded by the presently preserved assemblage.

In contrast to HC8, sample HC7 records a much lower pressure. The sample contains ~ 3–12 vol.% (average 8 vol.%) garnet, which for the modelled bulk composition implies pressures of around 5 kbar. Therefore, although Takamura et al. (2015) did not report reaction microstructures from HC7, this sample has much less garnet in comparison to the nearby HC8 and may be a domain in which garnet has been largely removed. As a reference point, at the *P–T* conditions recorded by HC8, sample HC7 would have had approximately 30 vol.% (33 mol.%) garnet.

The *P–T* conditions inferred here for HC7 and HC8 differ from those suggested by Takamura et al. (2015), who concluded the rocks reached 10.5–11 kbar and 900–950 ºC. However, Takamura et al. (2015) modelled the mineral assemblages to have free H_2O at temperatures greater than ca. 800 ºC, corresponding to hornblende breakdown. Free H_2O is at these temperatures in plagioclase–quartz bearing rocks is not realistic. Furthermore Takamura et al. (2015) did not use modal abundances as further constraints. In the modelling presented in this paper we incorporate melting of the rocks, which is a more realistic scenario than the presence of high-temperature free water, and additionally consider the modal abundances of critical minerals such as garnet to place additional constraints on the recorded *P–T* conditions.

Overall, mafic granulites in the EHC record peak conditions in excess of 850 ºC at pressures of 9–11 kbar, while rocks in the WHC record peak conditions at 800–850 ºC and pressure of 9–10 kbar. This corresponds to a high apparent thermal gradient of > 100–140 ºC $kbar^{-1}$. In sample HC8 garnet is mantled by symplectites of orthopyroxene and plagioclase, which represents either decreasing garnet modes within garnet-bearing fields or a univariant reaction in which garnet becomes unstable (White et al., 2002; Johnson and White, 2011). Either interpretation suggests that the retrograde *P–T* evolution for that sample is probably down-pressure-dominated, as such a trajectory involves decreasing garnet abundance and increasing abundance of orthopyroxene and plagioclase.

ACCEPTED MANUSCRIPT

In contrast, samples VC-HC-8/1, VC-HC-8/2 and VC-HC-8/3 from the EHC show no evidence for garnet decomposition microstructures. However, several other studies that incorporate samples from the EHC do show evidence of orthopyroxene and plagioclase after garnet, similar to rocks in the WHC (Schenk et al., 1991; Schumacher and Faulhaber, 1994). Schumacher and Faulhaber, (1994) determined that mafic granulites in the HC initially developed garnet coronas around peak orthopyroxene prior to the development of later orthopyroxene and plagioclase at the expense of garnet. This was interpreted to reflect a period of cooling followed by exhumation.

Existing conventional thermobarometry constraints from mafic granulites in the WHC yields variable *P–T* results. Osanai et al. (2016) obtained extremely high *P–T* conditions of ~17 kbar and 1035 °C, whereas Sajeev et al. (2007) reported peak metamorphism with *P–T* conditions of ~12.5 kbar and 844–982 °C for a similar lithology. Takamura et al. (2015) calculated pseudosections for mafic granulites in similar locations as previous studies. The peak *P–T* conditions they calculated are significantly lower than those from Osanai et al. (2016).

5.1.2. Comparison with metasedimentary rocks

The *P–T* conditions and metamorphic evolution of the UHT pelitic granulites from the HC have been extensively studied in the past two decades using both conventional thermobarometry and calculated phase equilibria modelling. The *P–T* evolutions of the Highland Complex from previous studies are summarised in Table 1. Our modelling of mafic granulites in the WHC supports a down-pressure retrograde *P–T* trajectory, consistent with previous studies that infer near-isothermal decompression in the WHC (Schenk et al., 1991; Faulhaber and Raith, 1991; Hiroi et al., 1994; Raase and Schenk, 1994; Kriegsman and Schumacher, 1999; Sajeev and Osanai, 2004b, 2004a, Osanai et al., 2006, 2016a, Sajeev et al., 2007, 2010, Dharmapriya et al., 2014, 2015b, 2017; Takamura et al., 2015). There are comparatively fewer metamorphic studies that use phase equilibria modelling from the EHC. Fernando et al. (2003) reported no evidence for down-pressure-related reaction microstructures in garnet–biotite gneiss and charnockite and interpreted a slow cooling-dominated retrograde history. Mathavan and Fernando (2001) also reported evidence for near-isobaric cooling based on the reaction of scapolite + quartz producing garnet in Maligawila calc-silicate granulites in the easternmost HC. Therefore, the limited petrological evidence from metasedimentary rocks supports a cooling-dominated retrograde trajectory after peak metamorphism.

It is interesting as to why some rocks from the Highland Complex appear to contain cooling-dominated reaction textures, whereas others have down-pressure dominated textures.

ACCEPTED MANUSCRIPT

To some extent this may be controlled by bulk compositions which are insensitive to parts of the *P–T* evolution. However, this is unlikely to be case with the mafic rocks from the EHC modelled in this study, which should record a decrease in garnet mode during high-temperature pressure drop as recorded by mafic garnet decomposition microstructures elsewhere in the EHC (Schenk et al., 1991; Schumacher and Faulhaber, 1994). Potentially variations in rock reactivity may have been controlled by variations in melt content, although the garnet-decomposition textures are nominally anhydrous. Nonetheless melt-bearing rocks are generally perceived to be more reactive than melt-free rocks (Brown, 2002; White and Powell, 2002; Morrissey et al., 2016). Irrespective of the reasons for variable rock reactivity, it is likely that many rocks from the Highland Complex only record small parts of the *P–T* evolution, as was suggested for effectively anhydrous rocks from the Eastern Ghats Province (e.g. Kelsey et al., 2017).

5.2 Interpretation of zircon U–Pb age data and implications for the thermal history of the Highland Complex

Kitano et al. (2018) and Osanai et al. (2016b) have collected extensive zircon U–Pb datasets from the Highland Complex. Fig. 9 shows a compilation of these data using samples from metasedimentary rocks, mafic granulites and orthopyroxene-bearing felsic gneisses that appear to have old (> 1500 Ma) detrital zircon or protolith age or metasedimentary samples that now have no record of old zircons. For samples that have old age populations, isotopic disturbance at around 600–500 Ma will lead to discordant grains that distinctly lie off concordia. Therefore concordant analyses from these samples between ca. 600–500 Ma probably represent complete Pb loss or growth of new zircon during metamorphism.

Figure 9 shows analyses that are between 99–101% concordant. It is evident there is continuum of zircon ages between ca. 650–460 Ma. Within this continuum, individual samples also contain a continuous range of concordant ages that span at least 100 Ma (Kitano et al., 2018; Osanai et al., 2016b). The data can be interpreted in several ways. It may represent the interference between distinct metamorphic events at ca. 650 Ma and 460 Ma, with the continuum of ages recording partial Pb loss from the older population. Alternatively, the continuum of zircon ages may reflect a prolonged period of high-grade metamorphism where zircon growth in individual rocks was controlled by melt–rock interaction.

Among the data collected in the present study, except for the two discordant older ages, which are interpreted to be inherited zircon with later Pb modification, the metamorphic zircon ages range between ca. 660–520 Ma (Fig. 6a). In this study, D_{REE} zircon/garnet values for

ACCEPTED MANUSCRIPT

660–560 Ma zircons are close to unity. A variety of empirical studies of high-grade terranes suggest that simultaneous growth of zircon and garnet will result in D_{REE} values of ~1 for the middle to heavy REE with a slightly concave-up distribution pattern (MREE likely to slightly favour garnet, and the HREE 1:1 or favouring zircon) (Whitehouse and Platt, 2003; Hokada and Harley, 2004; Kelly and Harley, 2005; Harley and Kelly, 2007; Taylor et al., 2015a, 2017). D_{HREE} zircon/garnet values of ~1, representing equilibrium partitioning, are also supported by the experimental results of Taylor et al. (2015b). Therefore, the 660–520 Ma aged zircons in this study are interpreted to be metamorphic in origin and to have grown in equilibrium with garnet. The youngest group of zircon grains from sample VC-HC-8/1 at ca. 520 Ma have slightly higher D_{REE} zircon/garnet values, which might suggest HREE favouring zircon over garnet at a lower metamorphic temperature (e.g. Rubatto and Hermann 2007), or fluid modification of zircon (e.g. Taylor et al., 2014; Zhong et al., 2018). Notably, all the recent geochronology studies of mafic granulites from both the EHC and WHC show similar continuous age ranges with similar Th/U characteristics to the data in our study. The lowest Th/U ratios are observed at the start of the age spread at ca. 660–630 Ma, with an increase in the Th/U ratios to younger ages (Fig. 6a) (Sajeev et al., 2007; Takamura et al., 2015). Rubatto (2017) suggests that coexisting Th-rich phases such as allanite are the reason for the low Th/U ratio in metamorphic zircon in eclogite, amphibolite and granulite facies rocks. The absence of these phases in some rocks (either by dissolution in melt, or because of composition) produces metamorphic zircon with higher Th/U ratios. The increase in Th/U ratios with decreasing age may suggest progressive dissolution of these minerals during long-lived metamorphism between 660–520 Ma.

Several studies (Santosh et al., 2014; Dharmapriya et al., 2015b, 2016, Takamura et al., 2015, 2016; Osanai et al., 2016b) have suggested that the metamorphic history of the Highland Complex involves more than one thermal cycle. This is in part based on the presence of discrete zircon age populations in some samples. Conversely other studies (Sajeev et al., 2003, 2007) interpret the metamorphic history to have involved one long-lived event. Problematic for the interpretation of zircon age data from the Highland Complex is the near complete lack of zircon trace element compositional data that allows zircon ages to be linked to the bulk silicate mineralogy that defines the *P–T* evolution. Until a comprehensive petrochronological dataset exists, the interpretation of zircon U–Pb ages from the Highland Complex will remain problematic. Nonetheless, we suggest simply taking the weighted average of the metamorphic zircon ages to derive an apparently tightly constrained age for metamorphism is misleading. Instead, based on the range of zircon ages collected from Sample VC-HC-8/1 that appear to have grown or recrystallised in equilibrium with garnet, we interpret that the ages need not be true ages of zircon growth – they could be (at least in part)

ACCEPTED MANUSCRIPT

Pb loss from older grains, but they still indicate a prolonged event. Therefore, we interpret the spread of more than 100 Ma of concordant zircon ages (Fig. 9) to record the duration of high temperature conditions.

Similar long-lived high-grade metamorphism has been reported in other regions including the Eastern Ghats orogenic belt, India (>> 50Myr, up to 200 Myr, Korhonen et al., 2013), Trivandrum Block, Southern India (Taylor et al., 2014), Arunta region, central Australia (Morrissey et al., 2014), Musgrave Province, central Australia (Walsh et al., 2015) and southern Madagascar (Fitzsimons, 2016). In the Eastern Ghats orogenic belt, long-lived (> 50 Ma) cooling has been suggested on the basis of geochronological data (Korhonen et al., 2013). Allied to that apparent record of long-lived high-temperatures is a mineral reaction textural record of near isobaric cooling. To sustain long lived (> 50 Ma) high to ultrahigh temperatures in the crust requires prolonged regional-scale high heat flow. Notable in the Eastern Ghats orogenic belt is that volumetrically significant regions contain higher than average levels of crustal heat production (Kumar et al., 2007). As shown by Sandiford et al. (1998); Clark et al. (2011); and Horton et al. (2016), high rates of crustal heat production are almost certainly required to generate and sustain high and ultrahigh temperatures in the crust for extended periods of time. However, long-lived cooling can only occur if rocks reside at depth because pronounced exhumation will drive cooling irrespective of the magnitude of crustal heat production. Therefore, in such systems cooling at depth cannot occur rapidly.

The post-peak metamorphic textural record in mafic rocks in the Highland Complex indicates that initially garnet growth continued at the modal expense of peak orthopyroxene (Schenk et al., 1991; Schumacher and Faulhaber, 1994), suggesting a period of cooling at depth. This was subsequently overprinted by the formation of orthopyroxene and plagioclase at the expense of garnet (Schenk et al., 1991; Schumacher and Faulhaber, 1994). The rocks described by Schenk et al. (1991) and Schumacher and Faulhaber (1994) that record this post-peak garnet growth have not been modelled. However, based on mole percent contours of garnet in the range of bulk compositions modelled in this paper, retrograde garnet growth can occur along retrograde paths with dP/dT gradients as steep as 750 °C/GPa^{-1}. This means that modest pressure decrease during cooling will still lead to garnet growth. The subsequent breakdown of garnet suggests that the retrograde path evolved toward steeper dP/dT gradients. The duration of the cooling-dominated interval is not well constrained. Published *P–T* paths that depict this cooling-dominated interval convey the impression it was a comparatively minor part of the *P–T* evolution (e.g. Dharmapriya et al., 2017). However, *P–T* paths do not convey *T–time* and *P–time* histories.

ACCEPTED MANUSCRIPT

Some insight into the temperature–time evolution comes from garnet diffusion modelling (Fernando et al., 2003), which suggests the Highland Complex cooled from approximately peak conditions between 1–5 °C Ma^{-1}, with allied isotopic data pointing to cooling at 2–3 °C Ma^{-1}. Such slow cooling at high temperatures can only occur if high heat flow is maintained. This either requires a sustained magmatic flux through the terrane and/or maintenance of a thin lithosphere and/or high rates of crustal heat production. There is little geological evidence for a volumetrically significant external magmatic flux during high temperature metamorphism in the Highland Complex. Additionally, geophysical studies (Tantrigoda and Geekiyanage, 2008) indicate the present-day Sri Lankan crust is between 31–37 km thick. This constraint, combined with the lack of major post-Cambrian crustal thickening events and the presence of 8–10 kbar rocks at the surface, implies the crust was not significantly thinned during metamorphism. Therefore, the existence of long-lived high temperatures implied by diffusional modelling (Fernando et al., 2003), and the age record of zircon growth probably reflects a significant contribution from crustal heat production. Support for this notion comes from the Kerala Khondalite Belt (KKB) in Southern India, which numerous authors have asserted is a lithotectonic extension of the Highland Complex (Plavsa et al., 2014; Kitano et al., 2018). Ray et al. (2008) showed the KKB has significantly elevated rates of crustal heat production. If the Highland Complex and KKB are parts of the same lithotectonic belt, it is likely the Highland Complex also has higher than average crustal heat production. Furthermore, Taylor et al. (2014) interpreted the KKB to have experienced long-lived high-temperature conditions similar to those proposed for the Highland Complex.

The modelling by Fernando et al. (2003) suggests slow high-temperature cooling was terminated by a 5- to 10-fold increase in cooling rate. While diffusional temperature–time modelling does not provide a unique solution, based on existing geochronological data they suggested this accelerated cooling began at around 480 Ma. This age is virtually identical to the youngest zircon ages in the combined data set shown in Fig. 9. We suggest dramatically increased cooling of the Highland Complex was driven by accelerated exhumation that began at around 480–470 Ma. If accelerated cooling was driven by exhumation, logically the record of garnet decomposition throughout the Highland Complex (e.g. Schumacher and Faulhaber, 1994) is the metamorphic textural record of that fast cooling. Evidence that exhumation was fast comes from aluminous metapelites which locally show the presence of late-stage andalusite (Hiroi et al., 1994; Raase and Schenk, 1994), requiring the generation of upper crustal thermal gradients in excess of 40 °C km^{-1}. This is well in excess of the average thermal gradient attendant to peak metamorphic conditions and the inferred post-peak cooling history, implying exhumation was sufficiently rapid to advect significant heat into the mid–upper crust. In summary, we suggest the Highland Complex experienced granulite conditions for the order

ACCEPTED MANUSCRIPT

of ca. 100 Myr. Thermobarometrically minor post-peak cooling (e.g. Dharmapriya et al., 2017) in fact probably represents a very long-lived temperature–time evolution, highlighting that *P–T* paths without temporal constraints are of little use in tectonic analysis.

6. Conclusions

1. The Highland Complex in Sri Lanka records high-grade metamorphism throughout its entirety. Garnet and zircon REE data suggest long-lived UHT metamorphism that may have begun as early as ca. 660 Ma, and continued until ca. 520 Ma. Further, a compilation of existing U–Pb data extends this duration to ca. 660–480 Ma.
2. *P–T* conditions estimated from calculated mineral equilibria forward modelling of mafic granulites in the western Highland Complex are down-pressure dominated. The eastern HC reached peak pressures of 8–9.5 kbar and temperatures of 870–970 °C, and records a lack of evidence for changing garnet modes, consistent with a cooling-dominated path. In the eastern and western Highland Complex the microstructural record of retrograde mineral growth is different, with mineral textures recording both near-isobaric cooling and pressure decrease. These varying records are likely to reflect the temporal evolution in rock reactivity that result in recording different parts of the *P–T* evolution.
3. *P–T* paths from the Highland Complex suggest peak conditions were followed by near-isobaric cooling, followed by pronounced high-temperature pressure decrease. However, diffusion modelling (Fernando et al., 2003) suggests slow post-peak cooling, which combined with zircon U–Pb geochronology implies rocks remained at depth for more than 50 Myr.
4. We suggest the apparently minor cooling interval from *P–T* analysis is in fact is the temporally dominant part of the *P–T* evolution in the Highland Complex. This highlights that without temporal constrains, *P–T* paths need to be treated with care in the analysis of tectonic systems.

Acknowledgments

We thank Prof. Guochun Zhao, Editor, referees Dr. Vinod Samuel, Prof. Somnath Dasgupta and Prof. Ian Fitzsimons for their constructive suggestions and comments which greatly improved our work. Special thanks to Prof. Ian Fitzsimons for his very careful and constructive reviews and comments. We thank Dr. Sarah Gilbert from Adelaide Microscopy for her much-appreciated assistance with LA–ICP–MS analysis. Funding for this study came from a Grant-in-Aid for Scientific Research (B) from Japan Society for the Promotion of Science (JSPS) to Toshiaki Tsunogae (Grant No. 26302009, Grant No. 26302009 and No. 18H01300), the Foreign Expert funding to M. Santosh at the China University of Geosciences Beijing, China and Professorial Fellow grant at the University of Adelaide, Australia. This study forms part of

ACCEPTED MANUSCRIPT

Xiao-Fang He's doctoral research at the China University of Geosciences Beijing and at the University of Adelaide, Australia, supported by the Chinese Scholarship Council (Grant No. 201606400003) and the Fundamental Research Funds for the Central Universities (Grant No. 2652017018).

References

Archibald, D.B., Collins, A.S., Foden, J.D., Razakamanana, T., 2017. Tonian Arc Magmatism in Central Madagascar: The Petrogenesis of the Imorona-Itsindro Suite. J. Geol. 125, 000–000. https://doi.org/10.1086/691185

Braun, I., Kriegsman, L.M., 2003. Proterozoic crustal evolution of southernmost India and Sri Lanka. Geol. Soc. London, Spec. Publ. 206, 169–202. https://doi.org/10.1144/GSL.SP.2003.206.01.10

Brown, M., 2002. Retrograde processes in migmatites and granulites revisited. J. Metamorph. Geol. 20, 25–40. https://doi.org/10.1046/j.0263-4929.2001.00362.x

Burton, K., O'Nions, R., 1990. Fe-Ti oxide chronometry: with application to granulite formation. Geochim. Cosmochim. Acta 54, 2593–2602.

Clark, C., Fitzsimons, I.C.W., Healy, D., Harley, S.L., 2011. How does the continental crust get really hot? Elements 7, 235–240. https://doi.org/10.2113/gselements.7.4.235

Cooray, P.G., 1994. The Precambrian of Sri Lanka: a historical review. Precambrian Res. 66, 3–18.

Dharmapriya, P.L., Malaviarachchi, S.P.K., Galli, A., Su, B.X., Subasinghe, N.D., Dissanayake, C.B., 2015a. Rare evidence for formation of garnet+corundum during isobaric cooling of ultrahigh temperature metapelites: New insights for retrograde P-T trajectory of the Highland Complex, Sri Lanka. Lithos 220–223, 300–317. https://doi.org/10.1016/j.lithos.2015.01.015

Dharmapriya, P.L., Malaviarachchi, S.P.K., Galli, A., Su, B.X., Subasinghe, N.D., Dissanayake, C.B., Nimalsiri, T.B., Zhu, B., 2014. P-T evolution of a spinel+quartz bearing khondalite from the Highland Complex, Sri Lanka: Implications for non-UHT metamorphism. J. Asian Earth Sci. 95, 99–113. https://doi.org/10.1016/j.jseaes.2014.05.003

Dharmapriya, P.L., Malaviarachchi, S.P.K., Kriegsman, L.M., Galli, A., Sajeev, K., Zhang, C., 2017. New constraints on the P–T path of HT/UHT metapelites from the Highland Complex of Sri Lanka. Geosci. Front. 8, 1405–1430. https://doi.org/10.1016/j.gsf.2016.12.005

Dharmapriya, P.L., Malaviarachchi, S.P.K., Sajeev, K., Zhang, C., 2016. New LA-ICPMS U–Pb ages of detrital zircons from the Highland Complex: insights into late Cryogenian to early Cambrian (ca. 665–535 Ma) linkage between Sri Lanka and India. Int. Geol. Rev. 58, 1856–1883. https://doi.org/10.1080/00206814.2016.1185650

Dharmapriya, P.L., Malaviarachchi, S.P.K., Santosh, M., Tang, L., Sajeev, K., 2015b. Late-Neoproterozoic ultrahigh-temperature metamorphism in the Highland Complex, Sri Lanka. Precambrian Res. 271, 311–333. https://doi.org/10.1016/j.precamres.2015.10.010

Ellis, D.J., Hiroi, Y., 1997. Secondary siderite-oxide-sulphide and carbonate-andalusite assemblages in cordierite granulites from Sri Lanka: post-granulite facies fluid evolution during uplift. Contrib. to Mineral. Petrol. 127, 315–335. https://doi.org/10.1007/s004100050283

Faulhaber, S., Raith, M., 1991. Geothermometry and Geobarometry of High-Grade Rocks: A Case Study on Garnet-Pyroxene Granulites in Southern Sri Lanka. Mineral. Mag. 55, 33–56. https://doi.org/10.1180/minmag.1991.055.378.04

Fernando, G.W.A.R., Hauzenberger, C.A., Baumgartner, L.P., Hofmeister, W., 2003. Modeling of retrograde diffusion zoning in garnet: Evidence for slow cooling of granulites from the Highland complex of Sri Lanka. Mineral. Petrol. 78, 53–71. https://doi.org/10.1007/s00710-002-0224-1

ACCEPTED MANUSCRIPT

Fitzsimons, I.C.W., 2016. Pan–African granulites of Madagascar and southern India: Gondwana assembly and parallels with modern Tibet. J. Mineral. Petrol. Sci. 111, 73–88. https://doi.org/10.2465/jmps.151117

Green, E.C.R., White, R.W., Diener, J.F.A., Powell, R., Holland, T.J.B., Palin, R.M., 2016. Activity-composition relations for the calculation of partial melting equilibria in metabasic rocks. J. Metamorph. Geol. 845–869. https://doi.org/10.1111/jmg.12211

Griffin, W.L., Belousova, E.A., Shee, S.R., Pearson, N.J., O'Reilly, S.Y., 2004. Archean crustal evolution in the northern Yilgarn Craton: U-Pb and Hf-isotope evidence from detrital zircons. Precambrian Res. 131, 231–282. https://doi.org/10.1016/j.precamres.2003.12.011

Guillong, M., Hametner, K., Reusser, E., Wilson, S. a, Günther, D., 2005. Preliminary characterisation of new glass reference materials (GSA-1G, GSC-1G, GSD-1G and GSE-1G) by laser ablation-inductively coupled plasma-mass spectrometry using 193 nm, 213 nm and 266 nm wavelengths. Geostand. Geoanalytical Res. 29, 315–331. https://doi.org/10.1111/j.1751-908X.2005.tb00903.x

Hapuarachchi, D., 1968. Cordierite and wollastonite-bearing rocks of south-western Ceylon. Geol. Mag. 105, 317–324. https://doi.org/10.1017/S0016756800054340

Harley, S.L., Kelly, N.M., 2007. The impact of zircon-garnet REE distribution data on the interpretation of zircon U-Pb ages in complex high-grade terrains: An example from the Rauer Islands, East Antarctica. Chem. Geol. 241, 62–87. https://doi.org/10.1016/j.chemgeo.2007.02.011

He, X.F., Santosh, M., Tsunogae, T., Malaviarachchi, S.P.K., Dharmapriya, P.L., 2016. Neoproterozoic arc accretion along the "eastern suture" in Sri Lanka during Gondwana assembly. Precambrian Res. 279, 57–80. https://doi.org/10.1016/j.precamres.2016.04.006

Hiroi, Y., Ogo, Y., Namba, K., 1994. Evidence for prograde metamorphic evolution of Sri Lankan pelitic granulites, and implications for the development of continental crust. Precambrian Res. 66, 245–263. https://doi.org/10.1016/0301-9268(94)90053-1

Hokada, T., Harley, S.L., 2004. Zircon growth in UHT leucosome: constraints from zircon-garnet rare earth elements (REE) relations in Napier Complex, East Antarctica. J. Mineral. Petrol. Sci. 99, 180–190. https://doi.org/10.2465/jmps.99.180

Holland, T.J.B., Powell, R., 2011. An improved and extended internally consistent thermodynamic dataset for phases of petrological interest, involving a new equation of state for solids. J. Metamorph. Geol. 29, 333–383. https://doi.org/10.1111/j.1525-1314.2010.00923.x

Horstwood, M.S.A., Košler, J., Gehrels, G., Jackson, S.E., Mclean, N.M., Paton, C., Pearson, N.J., Sircombe, K., Sylvester, P., Vermeesch, P., Bowring, J.F., Condon, D.J., Schoene, B., 2016. Community-Derived Standards for LA-ICP-MS U-(Th-)Pb Geochronology - Uncertainty Propagation, Age Interpretation and Data Reporting. Geostand. Geoanalytical Res. 40, 311–332. https://doi.org/10.1111/j.1751-908X.2016.00379.x

Horton, F., Hacker, B., Kylander-clark, A., Holder, R., Jöns, N., 2016. Focused radiogenic heating of middle crust caused ultrahigh temperatures in southern Madagascar 293–314. https://doi.org/10.1002/2015TC004040.Received

Jackson, S.E., Pearson, N.J., Griffin, W.L., Belousova, E.A., 2004. The application of laser ablation-inductively coupled plasma-mass spectrometry to in situ U-Pb zircon geochronology. Chem. Geol. 211, 47–69. https://doi.org/10.1016/j.chemgeo.2004.06.017

Jochum, K.P., Weis, U., Stoll, B., Kuzmin, D., Yang, Q., Raczek, I., Jacob, D.E., Stracke, A., Birbaum, K., Frick, D.A., Günther, D., Enzweiler, J., 2011. Determination of reference values for NIST SRM 610-617 glasses following ISO guidelines. Geostand. Geoanalytical Res. 35, 397–429. https://doi.org/10.1111/j.1751-908X.2011.00120.x

Johnson, T.E., White, R.W., 2011. Phase equilibrium constraints on conditions of granulite-facies metamorphism at Scourie, NW Scotland. J. Geol. Soc. London. 168, 147–158. https://doi.org/10.1144/0016-76492010-069

ACCEPTED MANUSCRIPT

Katz, M., 1972. Facies series of the high grade metamorphic rocks of the Ceylon Precambrian, in: Proc. 24th Int. Geol. Congr., Montreal. pp. 43–51.
Katz, M., 1971. The Precambrian metamorphic rocks of Ceylon. Geol. Rundschau.
Kehelpannala, K.V.W., 2004. Arc Accretion Around Sri Lanka During the Assembly of Gondwana. Gondwana Res. 7, 41–46.
Kehelpannala, K.V.W., 2003. Structural evolution of the middle to lower crust in Sri Lanka. J. Geol. Soc. Sri Lanka 11, 45–85.
Kelly, N.M., Harley, S.L., 2005. An integrated microtextural and chemical approach to zircon geochronology: Refining the Archaean history of the Napier Complex, east Antarctica. Contrib. to Mineral. Petrol. 149, 57–84. https://doi.org/10.1007/s00410-004-0635-6
Kitano, I., Osanai, Y., Nakano, N., Adachi, T., Fitzsimons, I.C.W., 2018. Detrital zircon and igneous protolith ages of high-grade metamorphic rocks in the Highland and Wanni Complexes, Sri Lanka: Their geochronological correlation with southern India and East Antarctica. J. Asian Earth Sci. 156, 122–144. https://doi.org/10.1016/j.jseaes.2018.01.017
Korhonen, F.J., Clark, C., Brown, M., Bhattacharya, S., Taylor, R., 2013. How long-lived is ultrahigh temperature (UHT) metamorphism? Constraints from zircon and monazite geochronology in the Eastern Ghats orogenic belt, India. Precambrian Res. 234, 322–350. https://doi.org/10.1016/j.precamres.2012.12.001
Kriegsman, L.M., Schumacher, J.C., 1999. Petrology of sapphirine-bearing and associated granulites from central Sri Lanka. J. Petrol. 40, 1211–1239. https://doi.org/10.1093/petroj/40.8.1211
Kröner, A., Cooray, P.G., Vitanage, P.W., 1991. Lithotectonic subdivision of the Precambrian basement in Sri Lanka. Cryst. crust Sri Lanka, Part 1, Summ. Res. Ger. Lankan Consortium. 5–21.
Kröner, A., Jaeckel, P., 1994. Zircon ages from rocks of the Wanni Complex, Sri Lanka. J. Geol. Soc. Sri Lanka 5, 41–57.
Kröner, A., Jaeckel, P., Williams, I.S., 1994. Pb-loss patterns in zircons from a high-grade metamorphic terrain as revealed by different dating methods: U-Pb and Pb-Pb ages for igneous and metamorphic zircons from northern Sri Lanka. Precambrian Res. 66, 151–181. https://doi.org/10.1016/0301-9268(94)90049-3
Kröner, A., Kehelpannala, K.V.W., Hegner, E., 2003. Ca. 750-1100 Ma magmatic events and Grenville-age deformation in Sri Lanka: Relevance for Rodinia supercontinent formation and dispersal, and Gondwana amalgamation. J. Asian Earth Sci. 22, 279–300. https://doi.org/10.1016/S1367-9120(03)00060-9
Kröner, A., Kehelpannala, K.V.W., Kriegsman, L.M., 1994. Origin of compositional layering and mechanism of crustal thickening in the high-grade gneiss terrain of Sri Lanka. Precambrian Res. 66, 21–37. https://doi.org/10.1016/0301-9268(94)90042-6
Kröner, A., Rojas-Agramonte, Y., Kehelpannala, K.V.W., Zack, T., Hegner, E., Geng, H.Y., Wong, J., Barth, M., 2013. Age, Nd-Hf isotopes, and geochemistry of the Vijayan Complex of eastern and southern Sri Lanka: A Grenville-age magmatic arc of unknown derivation. Precambrian Res. 234, 288–321. https://doi.org/10.1016/j.precamres.2012.11.001
Kumar, P.S., Menon, R., Reddy, G.K., 2007. The role of radiogenic heat production in the thermal evolution of a Proterozoic granulite-facies orogenic belt: Eastern Ghats, Indian Shield. Earth Planet. Sci. Lett. 254, 39–54. https://doi.org/10.1016/j.epsl.2006.11.018
Leake, B.E., Woolley, A.R., Arps, C.E., Birch, W.D., Gilbert, M.C., Grice, J.D., Hawthorne, F.C., Kato, A., Kisch, H.J., Krivovichev, V.G., Linthout, K., 1997. Nomenclature of Amphiboles: Report of the Subcommittee on Amphiboles of the International Mineralogical Association Commission on New Minerals and Mineral Names. Mineral. Mag. 61, 295–321.
Ludwig, K.R., 2012. ISOPLOT 3.75: A Geochronological Toolkit for Microsoft Excel. Berkeley Geochronol. Centre, Spec. Publ.
Malaviarachchi, S.P.K., Dharmapriya, P.L., 2015. Revisiting Ultrahigh Temperature granulites of Sri Lanka: New prograde and retrograde mineral textures from the

ACCEPTED MANUSCRIPT

Highland Complex. J. Indian Inst. Sci.
Mathavan, V., Fernando, G.W.A.R., 2001. Reactions and textures in grossular-wollastonite-scapolite calc-silicate granulites from Maligawila, Sri Lanka: Evidence for high-temperature isobaric cooling in the meta-sediments of the Highland Complex. Lithos 59, 217–232. https://doi.org/10.1016/S0024-4937(01)00057-3
Milisenda, C.C., Liew, T.C., Hofman, A.W., Kroner, A., 1988. Isotopic Mapping of Age Provinces in Precambrian High-Grade Terrains : Sri Lanka. J. Geol. 96, 608–615.
Morrissey, L.J., Hand, M., Kelsey, D.E., 2017. A curious case of agreement between conventional thermobarometry and phase equilibria modelling in granulites: New constraints on *P-T* estimates in the Antarctica segment of the Musgrave-Albany-Fraser-Wilkes Orogen. J. Metamorph. Geol. 35, 1023–1050. https://doi.org/10.1111/jmg.12266
Morrissey, L.J., Hand, M., Lane, K., Kelsey, D.E., Dutch, R.A., 2016. Upgrading iron-ore deposits by melt loss during granulite facies metamorphism. Ore Geol. Rev. 74, 101–121. https://doi.org/10.1016/j.oregeorev.2015.11.012
Osanai, Y., Sajeev, K., Nakano, N., Kitano, I., Kehelpannala, W.K., Kato, R., Adachi, T., Malaviarachchi, S.P., 2016a. UHT granulites of the Highland Complex, Sri Lanka I: Geological and petrological background. J. Mineral. Petrol. Sci. 111, 145–156. https://doi.org/10.2465/jmps.151227
Osanai, Y., Sajeev, K., Nakano, N., Kitano, I., Kehelpannala, W.K., Kato, R., Adachi, T., Malaviarachchi, S.P., 2016b. UHT granulites of the Highland Complex, Sri Lanka II: Geochronological constraints and implications for Gondwana correlation. J. Mineral. Petrol. Sci. 111, 157–169. https://doi.org/10.2465/jmps.151227
Osanai, Y., Sajeev, K., Owada, M., Kehelpannala, K.V.W., Prame, W.K.B., Nakano, N., Jayatileke, S., 2006. Metamorphic evolution of high-pressure and ultrahigh-temperature granulites from the Highland Complex, Sri Lanka. J. Asian Earth Sci. 28, 20–37. https://doi.org/10.1016/j.jseaes.2004.09.013
Osanai, Y., Tsutomu, A.K., Miyashita, Y., Kusachi, I., Yamasaki, T., Doyama, D., Prame, W.K.B.N., Jayatileke, S., Mathavan, V., 2000. Geological fieldwork in the southwestern and central parts of the highland complex, Sri Lanka, during 1998-1999, with special reference to the highest grade metamorphic rocks. J. Geosci. 43, 227–247.
Paton, C., Hellstrom, J., Paul, B., Woodhead, J., Hergt, J., 2011. Iolite: Freeware for the visualisation and processing of mass spectrometric data. J. Anal. At. Spectrom. 26, 2508. https://doi.org/10.1039/c1ja10172b
Pearce, M.A., White, A.J.R., Gazley, M.F., 2015. TCInvestigator: Automated calculation of mineral mode and composition contours for thermocalc pseudosections. J. Metamorph. Geol. 33, 413–425. https://doi.org/10.1111/jmg.12126
Perera, L.R.K., 1984. Co-existing cordierite-almandine-a key to the metamorphic history of Sri Lanka. Precambrian Res. 25, 349–364. https://doi.org/10.1016/0301-9268(84)90009-3
Plavsa, D., Collins, A.S., Payne, J.L., Foden, J.D., Clark, C., Santosh, M., 2014. Detrital zircons in basement metasedimentary protoliths unveil the origins of southern India. Bull. Geol. Soc. Am. 126. https://doi.org/10.1130/B30977.1
Prame, W., 1991. Metamorphism and nature of the granulite-facies crust in southwestern Sri Lanka: characterization by pelitic/psammopelitic rocks and associated. Summ. Res. Ger. Lankan Consort. 827, 188–199.
Raase, P., Schenk, V., 1994. Petrology of granulite-facies metapelites of the Highland Complex, Sri Lanka: implications for the metamorphic zonation and the P-T path. Precambrian Res. 66, 265–294. https://doi.org/10.1016/0301-9268(94)90054-X
Ray, L., Roy, S., Srinivasan, R., 2008. High radiogenic heat production in the Kerala Khondalite Block, Southern Granulite Province, India. Int. J. Earth Sci. 97, 257–267. https://doi.org/10.1007/s00531-007-0278-8
Rubatto, D., 2017. Zircon: the metamorphic mineral. Rev. Mineral. geochemistry 83. https://doi.org/10.2138/rmg.2017.83.10
Rubatto, D., Hermann, J., 2007. Experimental zircon/melt and zircon/garnet trace element partitioning and implications for the geochronology of crustal rocks. Chem. Geol. 241,

ACCEPTED MANUSCRIPT

38–61. https://doi.org/10.1016/j.chemgeo.2007.01.027
Sajeev, K., Osanai, Y., 2005. Thermal gradients in the Sri Lankan granulite terrane: A garnet-biotite thermometric approach. J. Metamorph. Geol. 23, 383–397. https://doi.org/10.1111/j.1525-1314.2005.00582.x
Sajeev, K., Osanai, Y., 2004b. Osumilite and spinel+quartz from Sri Lanka: Implications for UHT conditions and retrograde P-T path. J. Mineral. Petrol. Sci. 99, 320–327. https://doi.org/10.2465/jmps.99.320
Sajeev, K., Osanai, Y., 2004a. Ultrahigh-temperature Metamorphism (1150°C, 12 kbar) and Multistage Evolution of Mg-, Al-rich Granulites from the Central Highland Complex, Sri Lanka. J. Petrol. 45, 1821–1844. https://doi.org/10.1093/petrology/egh035
Sajeev, K., Osanai, Y., Connolly, J. a. D., Suzuki, S., Ishioka, J., Kagami, H., Rino, S., 2007. Extreme Crustal Metamorphism during a Neoproterozoic Event in Sri Lanka: A Study of Dry Mafic Granulites. J. Geol. 115, 563–582. https://doi.org/10.1086/519778
Sajeev, K., Osanai, Y., Suzuki, S., Kagami, H., 2003. Geochronological evidence for multistage-metamorphic events in ultrahigh-temperature granulites from central Highland Complex, Sri Lanka. Polar Geosci. 16, 137–148.
Sajeev, K., Williams, I.S., Osanai, Y., 2010. Sensitive high-resolution ion microprobe U-Pb dating of prograde and retrograde ultrahigh-temperature metamorphism as exemplified by Sri Lankan granulites. Geology 38, 971–974. https://doi.org/10.1130/G31251.1
Sandiford, M., Hand, M., McLaren, S., 1998. High geothermal gradient metamorphism during thermal subsidence. Earth Planet. Sci. Lett. 163, 149–165. https://doi.org/10.1016/S0012-821X(98)00183-6
Sandiford, M., Powell, R., Martin, S.F., Perera, L.R.K., 1988. Thermal and baric evolution of garnet granulites from Sri Lanka. J. Metamorph. Geol. 6, 351–364. https://doi.org/10.1111/j.1525-1314.1988.tb00425.x
Santosh, M., Tsunogae, T., Malaviarachchi, S.P.K., Zhang, Z., Ding, H., Tang, L., Dharmapriya, P.L., 2014. Neoproterozoic crustal evolution in Sri Lanka: Insights from petrologic, geochemical and zircon U-Pb and Lu-Hf isotopic data and implications for Gondwana assembly. Precambrian Res. 255, 1–29. https://doi.org/10.1016/j.precamres.2014.09.017
Schenk, V., Raase, P., Schumacher, R., 1991. Metamorphic zonation and PT history of the Highland Complex in Sri Lanka. Cryst. crust Sri Lanka, part I. 150–163.
Schumacher, R., Faulhaber, S., 1994. Summary and discussion of P-T estimates from garnet-pyroxene-plagioclase-quartz-bearing granulite-facies rocks from Sri Lanka. Precambrian Res. 66, 295–308. https://doi.org/10.1016/0301-9268(94)90055-8
Schumacher, R., Schenk, V., Raase, P., 1990. Granulite facies metamorphism of metabasic and intermediate rocks in the Highland Series of Sri Lanka, in: Ashworth, J.R., Brown, M. (Eds.), High-Temperature Metamorphism and Crustal Anatexis. pp. 235–271.
Sun, S. -s., McDonough, W.F., 1989. Chemical and isotopic systematics of oceanic basalts: implications for mantle composition and processes. Geol. Soc. London, Spec. Publ. 42, 313–345. https://doi.org/10.1144/GSL.SP.1989.042.01.19
Takahashi, K., Tsunogae, T., Santosh, M., Takamura, Y., Tsutsumi, Y., 2018. Paleoproterozoic (ca. 1.8 Ga) arc magmatism in the Lützow-Holm Complex, East Antarctica: Implications for crustal growth and terrane assembly in erstwhile Gondwana fragments. J. Asian Earth Sci. 157, 245–268. https://doi.org/10.1016/j.jseaes.2017.07.053
Takamura, Y., Tsunogae, T., Santosh, M., Malaviarachchi, S.P.K., Tsutsumi, Y., 2016. U-Pb geochronology of detrital zircon in metasediments from Sri Lanka: Implications for the regional correlation of Gondwana fragments. Precambrian Res. 281, 434–452. https://doi.org/10.1016/j.precamres.2016.06.015
Takamura, Y., Tsunogae, T., Santosh, M., Malaviarachchi, S.P.K., Tsutsumi, Y., 2015. Petrology and zircon U-Pb geochronology of metagabbro from the Highland Complex, Sri Lanka: Implications for the correlation of Gondwana suture zones. J. Asian Earth Sci. 113, 826–841. https://doi.org/10.1016/j.jseaes.2015.07.001
Takamura, Y., Tsunogae, T., Santosh, M., Tsutsumi, Y., 2018. Detrital zircon geochronology

ACCEPTED MANUSCRIPT

of the Lützow-Holm Complex, East Antarctica: Implications for Antarctica–Sri Lanka correlation. Geosci. Front. 9, 355–375. https://doi.org/10.1016/j.gsf.2017.08.006
Tantrigoda, D.A., Geekiyanage, P., 2008. A Preliminary Crustal Thickness Map of Sri Lanka. Journal-Geological Soc. India 71, 551.
Taylor, R.J.M., Clark, C., Fitzsimons, I.C.W., Santosh, M., Hand, M., Evans, N., McDonald, B., 2014. Post-peak, fluid-mediated modification of granulite facies zircon and monazite in the Trivandrum Block, southern India. Contrib. to Mineral. Petrol. 168, 1–17. https://doi.org/10.1007/s00410-014-1044-0
Taylor, R.J.M., Clark, C., Harley, S.L., Kylander-Clark, A.R.C., Hacker, B.R., Kinny, P.D., 2017. Interpreting granulite facies events through rare earth element partitioning arrays. J. Metamorph. Geol. 35, 759–775. https://doi.org/10.1111/jmg.12254
Taylor, R.J.M., Harley, S.L., Hinton, R.W., Elphick, S., Clark, C., Kelly, N.M., 2015. Experimental determination of REE partition coefficients between zircon, garnet and melt: A key to understanding high-T crustal processes. J. Metamorph. Geol. 33, 231–248. https://doi.org/10.1111/jmg.12118
White, R.W., Powell, R., 2002. Melt loss and the preservation of granulite facies mineral assemblages. J. Metamorph. Geol. 20, 621–632. https://doi.org/10.1046/j.1525-1314.2002.00206.x
White, R.W., Powell, R., Clarke, G.L., 2002. The interpretation of reaction textures in Fe-rich metapelitic granulites of the Musgrave Block, Central Australia: Constraints from mineral equilibria calculations in the system. J. Metamorph. Geol. 20, 41–55. https://doi.org/10.1046/j.0263-4929.2001.00349.x
Whitehouse, M.J., Platt, J.P., 2003. Dating high-grade metamorphism - Constraints from rare-earth elements in zircon and garnet. Contrib. to Mineral. Petrol. 145, 61–74. https://doi.org/10.1007/s00410-002-0432-z
Willbold, M., Hegner, E., Kleinschrodt, R., Stosch, H.G., Kehelpannala, K.V.W., Dulski, P., 2004. Geochemical evidence for a Neoproterozoic magmatic continental margin in Sri Lanka - Relevance for the Rodinia-Gondwana supercontinent cycle. Precambrian Res. 130, 185–198. https://doi.org/10.1016/j.precamres.2003.11.003
Zhong, S., Feng, C., Seltmann, R., Li, D., Qu, H., 2018. Can magmatic zircon be distinguished from hydrothermal zircon by trace element composition? The effect of mineral inclusions on zircon trace element composition. Lithos 315, 646–657. https://doi.org/10.1016/j.lithos.2018.06.029

Figure captions

Fig. 1 (a) Tectonic division map of Sri Lanka. (b) Geological map of the western Highland Complex (WHC) and (c) eastern Highland Complex (EHC) showing sample localities (after Cooray, 1994; Takamura et al., 2015; He et al., 2016).

Fig. 2 (a) Compiled *P–T* trajectories of high-T to UHT granulites from different localities of the Highland Complex with approximate sample locations shown. (b) Compiled existing *P–T* trajectories for mafic granulite. (c) Compiled existing *P–T* trajectories for leptynite (metasedimentary rock) from the Highland Complex (data from Schenk et al.,1991; Faulhaber and Raith, 1991; Raase and Schenk, 1994; Hiroi et al., 1994; Kriegsman and Schumacher, 1999; Mathavan and Fernando, 2001; Fernando et al., 2003; Sajeev and Osanai, 2004a, 2004b, Osanai et al., 2006, 2016; Sajeev et al., 2007, 2010; Dharmapriya et al., 2014, 2015b, 2017; Takamura et al.,2015).

Fig. 3 Outcrop photographs of the eastern Highland Complex sample locality. (a) mafic granulites in contact with country rocks; (b) massive texture of mafic granulites; (c) the

ACCEPTED MANUSCRIPT

plagioclase rich portion of studied mafic granulite; (d) garnet porphyroblast with amphibole and plagioclase-rich domains.

Fig. 4 Photomicrographs of studied samples from the eastern Highland Complex. (a) Garnet porphyroblast contains inclusions of clinopyroxene, orthopyroxene, plagioclase, ilmenite, and amphibole (sample VC-HC-8/1). (b) Hornblende occurs along the grain boundary between garnet and clinopyroxene (sample VC-HC-8/1, with LA–ICP–MS analysis spots shown). (c) Quartz inclusions in garnet porphyroblasts (sample VC-HC-8/1, BSE image). (d) Various inclusions in garnet porphyroblasts (sample VC-HC-8/2). (e) Amphibole, clinopyroxene and orthopyroxene in the matrix occurs as aggregates around garnet porphyroblasts (sample VC-HC-8/3). (f) Amphibole shows replacement microstructure of garnet, orthopyroxene clinopyroxene and plagioclase.

Fig. 5 Cathodoluminescence (CL) images for zircons from sample VC-HC-8/1. Spot numbers are also shown.

Fig. 6 (a) Tera-Wasserburg zircon U–Pb concordia plot for sample VC-HC-8/1. (b) Th/U ratios *vs.* $^{206}Pb/^{238}U$ age plot for compiled mafic granulite zircon age data. Data sourced from Sajeev et al. (2007); Takamura et al. (2015); Osanai et al. (2016b) and this study.

Fig. 7 (a) D_{REE} (zircon/ garnet) values for the REE and (b) D_{REE}(zircon/garnet) array plot in sample VC-HC-8/1 after Taylor et al. (2017), (c) Chondrite-normalised zircon REE plot and (d) Chondrite-normalised garnet REE plot. Normalizing values of chondrite are from Sun and McDonough (1989).

Fig. 8 Calculated *P–T* pseudosections for the studied samples using THERMOCALC. The bulk composition (in mol.%) is given above each pseudosection. Fields outlined in yellow are the interpreted peak fields and the red outline denotes where the peak fields of all three samples from the EHC overlap. Red and white dashed lines correspond to calculated contours for garnet (g) and clinopyroxene (cpx) mole percentages. (a) Sample VC-HC-8/1; (b) sample VC-HC-8/2; (c) sample VC-HC-8/3 with interpreted peak fields overlain. The shaded arrows in (a-c) represents a pressure decreasing cooling path parallel to garnet modal contours that correspond to the proportion of garnet in the samples. Garnet would not breakdown along this hypothetical PT path. d) and e) Sample HC8 and HC7. The star represents the inferred *P–T* conditions given by the preserved mineral assemblage. The thick purple dashed line is the *P–T* array from garnet-clinopyroxene thermometry. In e), the arrow represents the *P–T* evolution leading to the preserved assemblage assuming that HC7 and HC8 both experienced conditions of around 9 kbar and 830 °C.

Fig. 9 (a) A compilation of zircon U–Pb data from the Highland Complex for samples that have old (> 1500 Ma) protolith or zircon ages (data sourced from Osanai et al., 2016b and

ACCEPTED MANUSCRIPT

Kitano et al., 2018); (b) the continuum of concordant ages between ca. 650–460 Ma (n = 620); (c) shows the analyses in (b) plotted against concordia.

Table captions

Table 1 Summary of mineral reaction microstructures used to infer *P–T* path trajectories in studies on metapelitic and metabasic rocks from the Highland Complex. Black paths are from metapelitic rocks, red paths are from metabasic rocks

Supplementary materials

Supplementary material 1 Analytical methods

Supplementary Tables S1–S5

Table S1 Sample details and mineral modal abundance of mafic granulites in this study. Mineral abundances were determined by pixel counting of scanned thin section images in Photoshop.

Table S2 Representative electron microprobe analyses for minerals from sample VC-HC-8/1.

Table S3 LA–ICP–MS zircon U–Pb age data from sample VC-HC-8/1.

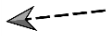
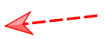
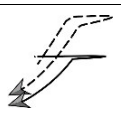
Table S4 Rare earth element (REE) composition of zircon and average garnet from sample VC-HC-8/1.

Table S5 Measured bulk-compositions for the studied samples and normalized compositions for each sample used for pseudosections.

Table S6 LA–ICP–MS garnet trace element data from sample VC-HC-8/1.

Fig. S1 (a) Zircon age vs. chondrite-normalised zircon Yb_N/Gd_N and (b) zircon age vs. zircon Yb_N plots. Normalizing values of chondrite are from Sun and McDonough (1989).

Table 1. ***Summary of mineral reaction microstructures used to infer P–T trajectories in studies on metapelitic and metabasic rocks from the Highland Complex.***

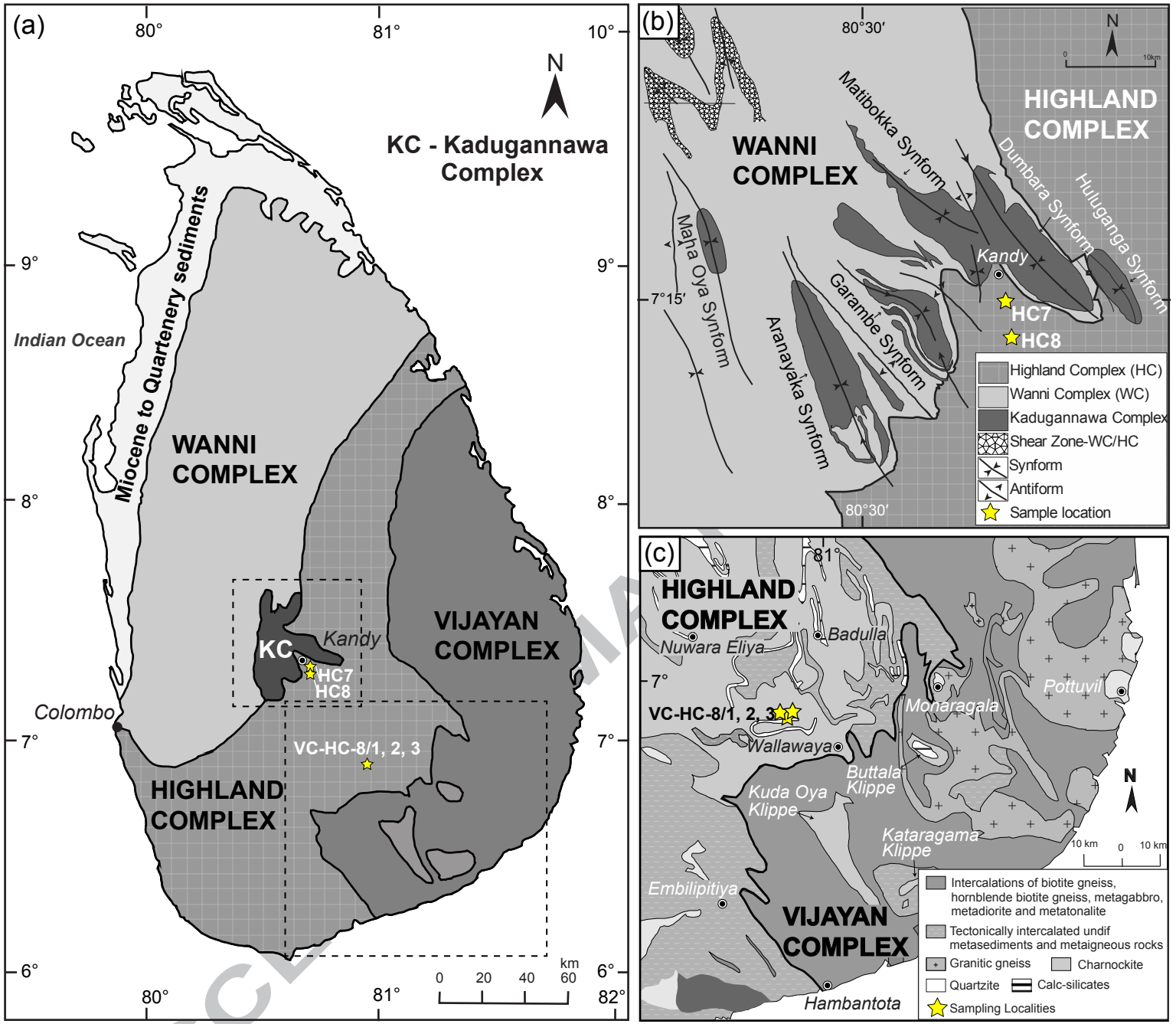
Study	Locality area	Zone	Reactant minerals	Product minerals	Field setting	Methods	*P–T* trajectory
Mathavan & Fernando (2001)	Maligawila at Buttala klippe	EHC	scp–wo	grt–qtz–cal	grossular–wollastonite–scapolite calc–silicate granulites	conventional thermobarometry	
Faulhaber & Raith (1991)	southeastern to sastern Highland Complex	EHC	opx–pl	grt–cpx–qtz	mafic granulites and charnockites interbedded with granulite-facies metasedimentary and metavolcanic rocks	conventional thermobarometry	
Fernando et al. (2003)	Rupaha	EHC	no information	no information	orthogneisses and charnockitic gneisses intercalated with metasediments	conventional thermobarometry	
Schenk et al. (1991)	southeastern to eastern Highland Complex	EHC	opx–pl	grt–cpx–qtz	both pelitic and mafic granulites	conventional thermobarometry	
Raase & Schenk (1994)	Puttalam and Kataragana, Colombo to Mahiyangana	WHC & EHC	bi–sill–qtz grt–sill–qtz grt–kfs grt–qtz	grt–crd–kfs crd bi–crd– qtz crd–opx	pelitic granulite layers intercalated in psammitic to semipelitic metasediments (garnet-biotite – hypersthene gneisses) or charnockitic rocks.	conventional thermobarometry	

ACCEPTED MANUSCRIPT

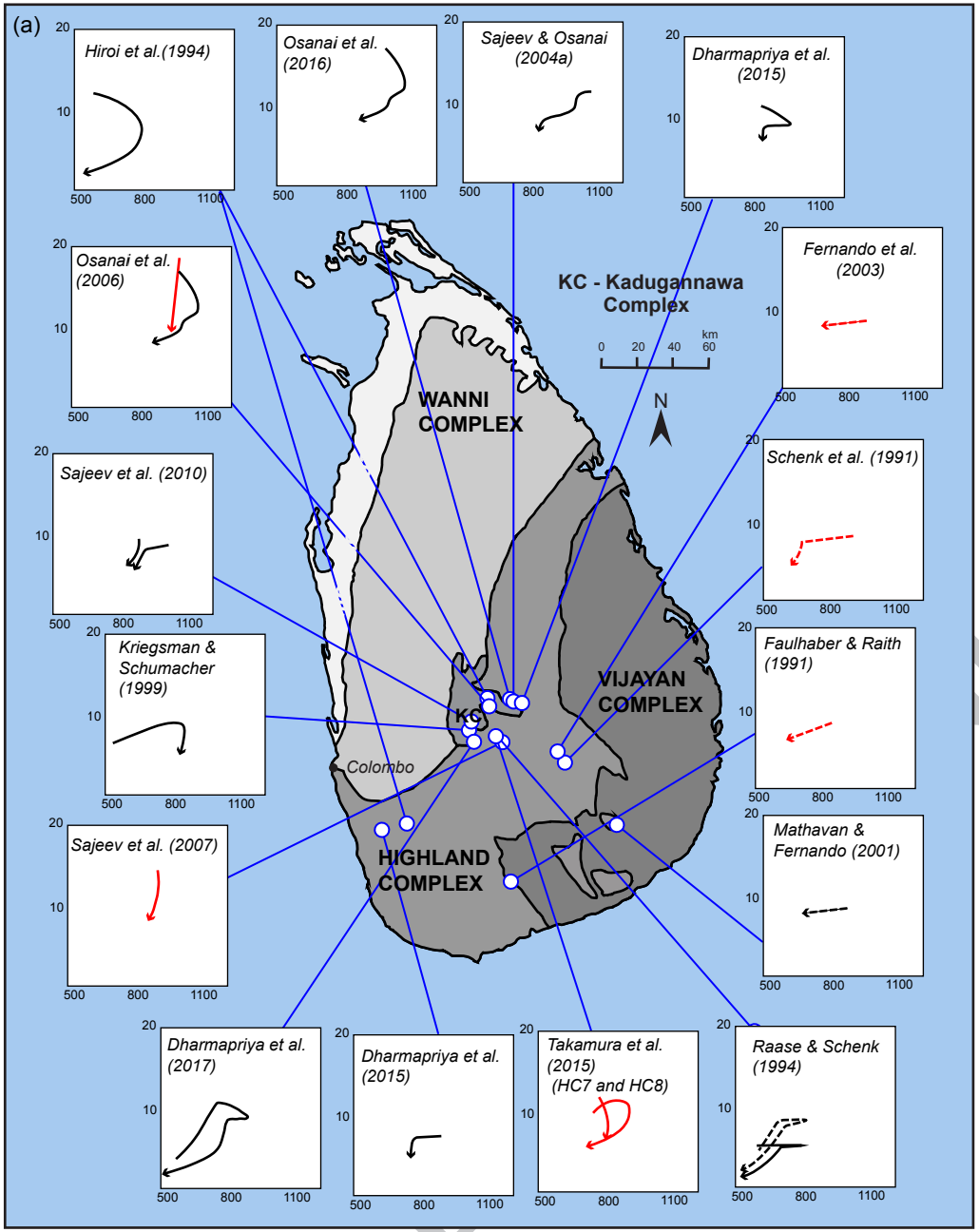
Takamura et al. (2015)	Hantana	WHC	grt–qtz	opx–pl	lenses of mafic granulites within foliated quartzite and psammitic–pelitic gneiss	**phase equilibria modelling** & conventional thermobarometry	
Osanai et al. (2006)	Victoria Dam, Gampola, Welimada, Nuwara Eliya	WHC	grt–cpx–qtz opx–cpx–pl	opx–pl hbl–qtz	leptynite; mafic granulites lenses within layered pelitic granulites and calc-silicate rocks;	conventional thermobarometry & petrogenetic grids	
Sajeev et al. (2007)	Victoria Dam near southeastern Kandy	WHC	grt–cpx–qtz	opx–pl	mafic granulites occur as lenses or blocks within layered pelitic granulites and calc-silicate rocks	conventional thermobarometry & petrogenetic grids	
Sajeev et al. (2010)	Talatuoya, Ampitiya and south Gampola	WHC	grt spr–qtz–opx grt	spr–opx grt spr–opx–sill	sapphirine bearing granulites interlayered with pelitic gneiss	conventional thermobarometry & **thermodynamic modelling**	
Dharmapriya et al. (2015)	Horana at southwestern Highland Complex	WHC	bi–sill	spl–qtz–kfs–melt	spinel- and cordierite-bearing garnet-sillimanite-biotite-graphite gneiss (khondalite) interbedded with intermediate granulites	**Phase equilibria modelling** & conventional thermobarometry	
Hiroi et al.(1994)	Western and Southwestern Highland Complex	WHC	ky crd–grt grt–sill–qtz	sill crn–ky–spr–grt–spl crd–sp–kfs	khondalites (graphitic garnet-sillimanite-K-feldspar-quartz gneisses); pelitic granulite	conventional thermobarometry	
Kriegsman & Schumacher, (1999)	Hakurutale and Munwatte near Kandy	WHC	opx–sill ± crn ± spr grt–crn–spl grt grt–crd	grt spr opx–sill–spr spr–crd	Ca-poor, Mg-rich pelitic granulites; sapphirine-bearing granulites lenses in a quartzite alternating with thin metapelitic layers	conventional thermobarometry	
Osanai et al. (2016)	Ampitiya, Hanguranketa, Talatuoya	WHC	spr–qtz grt–spr–sill opx–sill grt–qtz	opx–sill crd–spl crd–spl–grtrt opx–pl	Mg-Al rich granulite; mafic granulite; pelitic granulite; calc-silicates.	conventional thermobarometry & petrogenetic grids	
Sajeev and Osanai. (2004a)	Gampola, Talatuoya	WHC	spr–qtz grt–spr–sill opx–sill grt–qtz	opx–sill crd–spl crd–spl–grt opx–pl	Mg-Al rich granulite layers within migmatite and marble	conventional thermobarometry & petrogenetic grids	
Dharmapriya et al. (2015a)	Gampola, Kotmale, Nawalapitiya, Nildandahinna, Galaha	WHC	bt–sil–qtz bi–sill spl–sill hbl–pl–qtz grt–cpx–qtz	grt–kfs grt–spl–kfs grt–crn grt–cpx opx–pl	Mg-Al rich granulite (sapphirine-bearing); metapelites; mafic granulite	conventional thermobarometry & **phase equilibria modelling**	
Dharmapriya et al. (2017)	Gampola	WHC	ky crd–grt grt–sill–qtz	sill crn–ky–spr–grt–sp crd–sp–kfs	high Al khondalite (garnet–sillimanite–graphite gneisses) overlayed by thick quartzite layers	conventional thermobarometry & **phase equilibria modelling**	

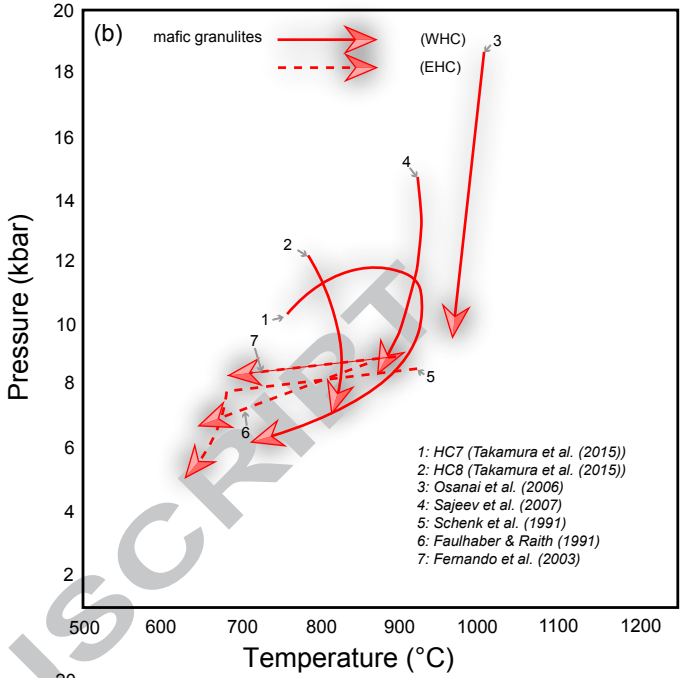
Mineral abbreviations follow Whitney and Evans, 2010

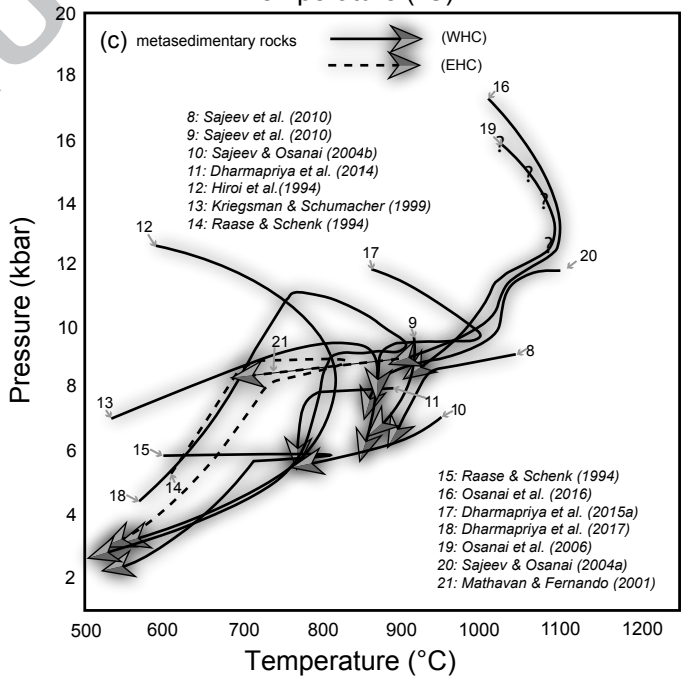
ACCEPTED MANUSCRIPT



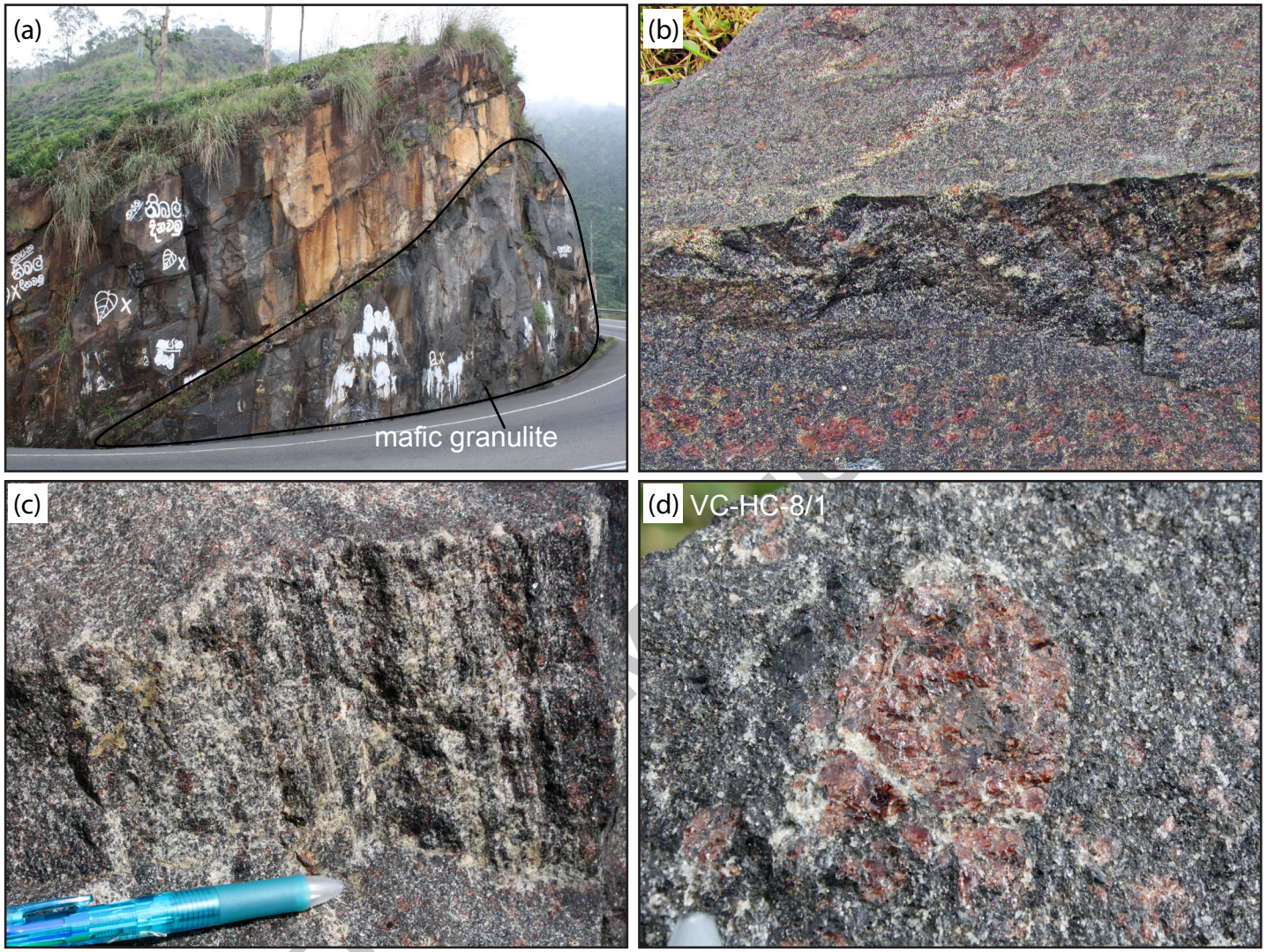
ACCEPTED MANUSCRIPT

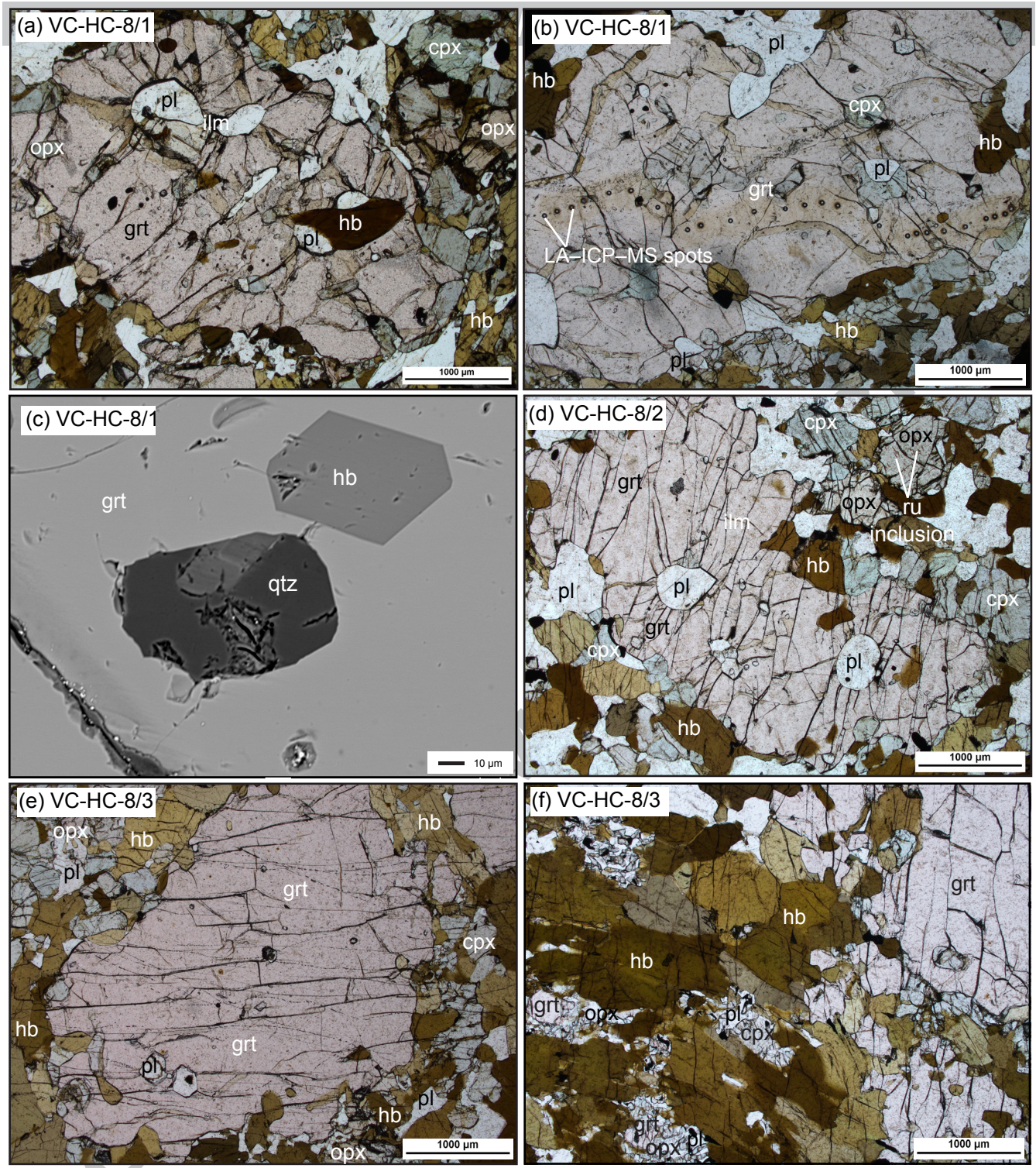




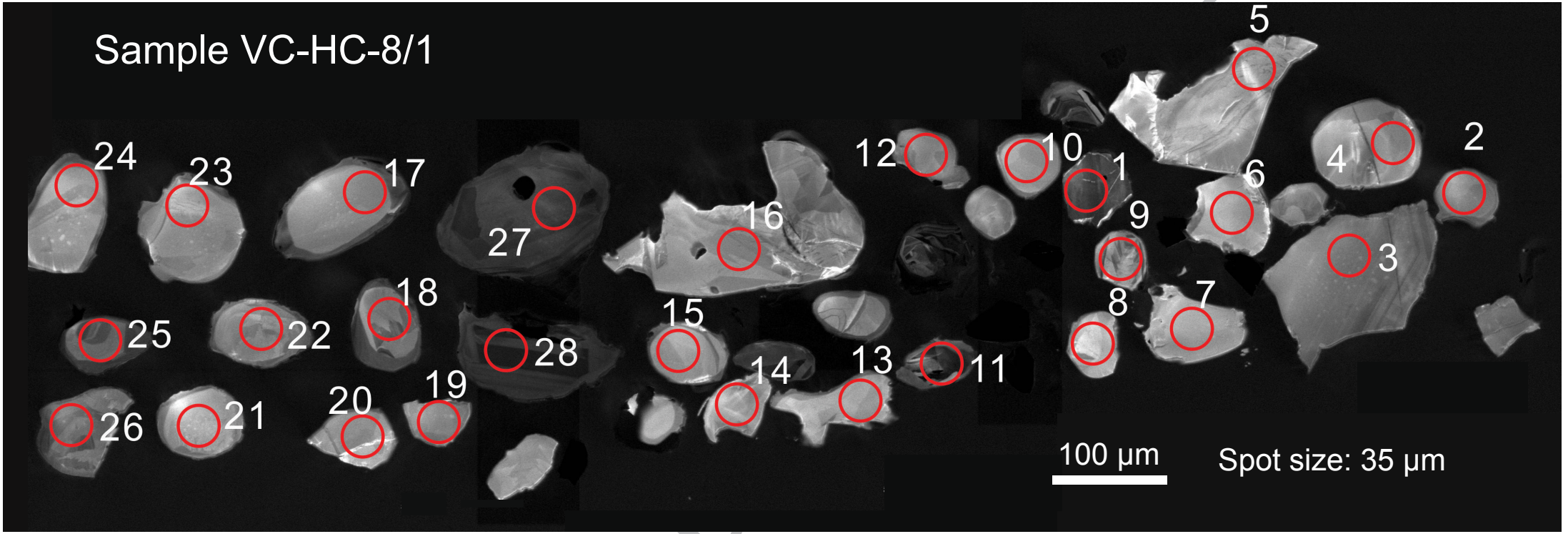


ACCEPTED MANUSCRIPT



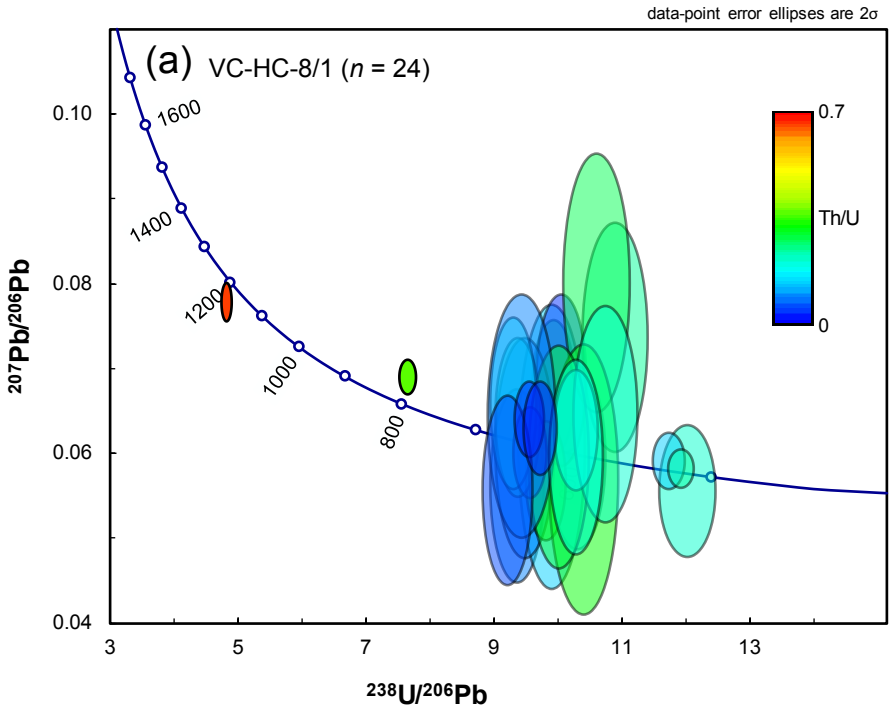

(a) VC-HC-8/1
cpx
pl
ilm
opx
opx
grt
hb
pl
hb
1000 µm
(b) VC-HC-8/1
pl
hb
cpx
hb
pl
grt
LA–ICP–MS spots
hb
pl
1000 µm
(c) VC-HC-8/1
hb
grt
qtz
10 µm
(d) VC-HC-8/2
cpx
opx
grt
opx
ru
inclusion
ilm
hb
pl
pl
cpx
grt
cpx
pl
hb
1000 µm
(e) VC-HC-8/3
opx
hb
hb
pl
grt
cpx
hb
grt
pl
pl
hb
opx
1000 µm
(f) VC-HC-8/3
grt
hb
hb
grt
opx
pl
cpx
grt
opx pl
1000 µm

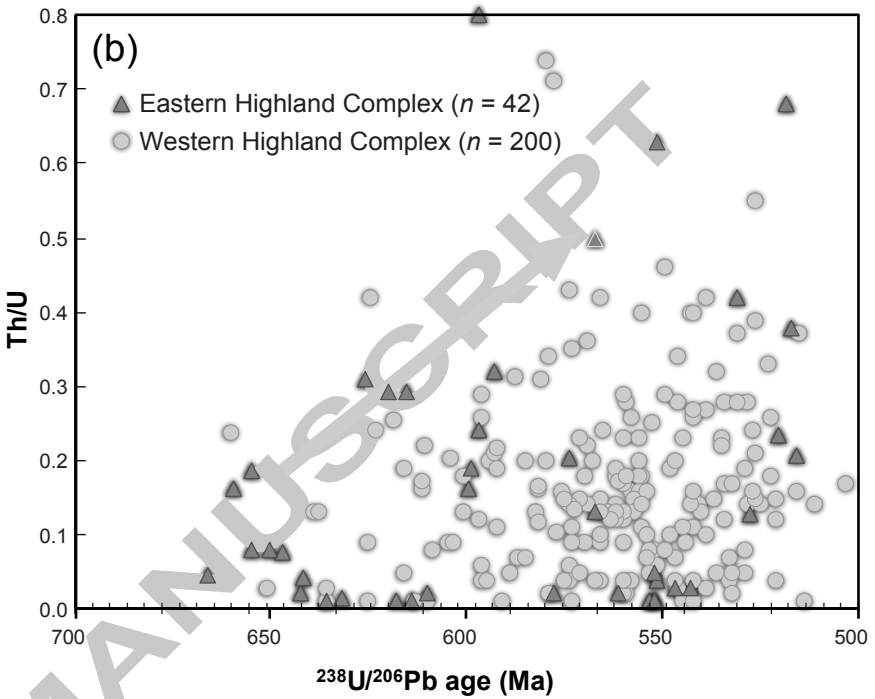
ACCEPTED MANUSCRIPT



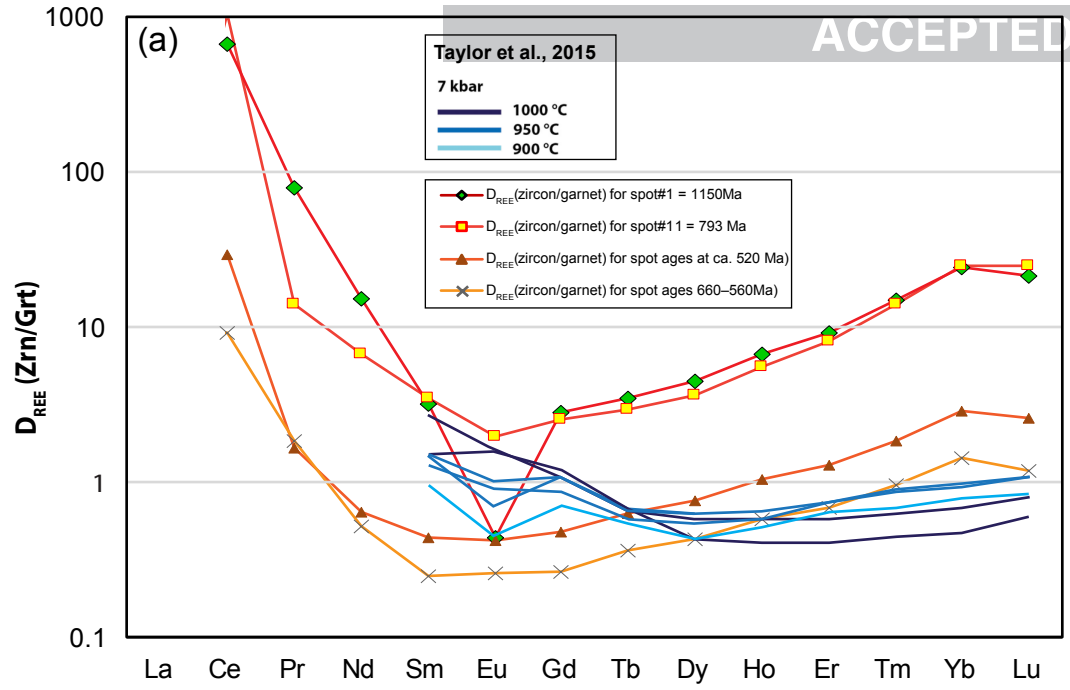
ACCEPTED

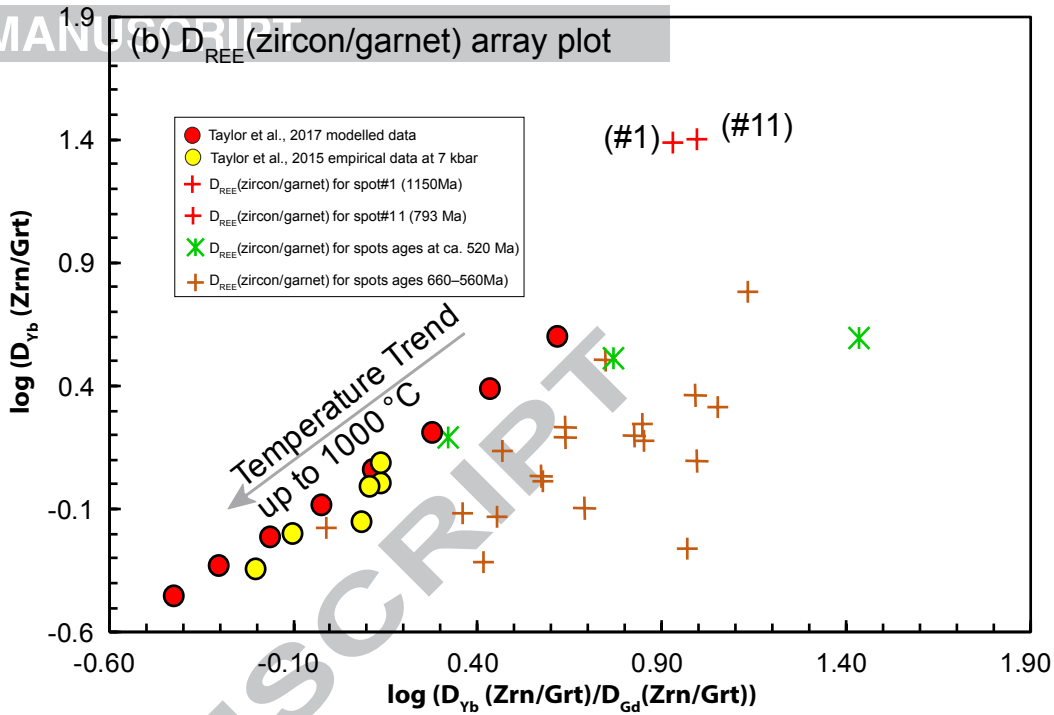
ACCEPTED MANUSCRIPT

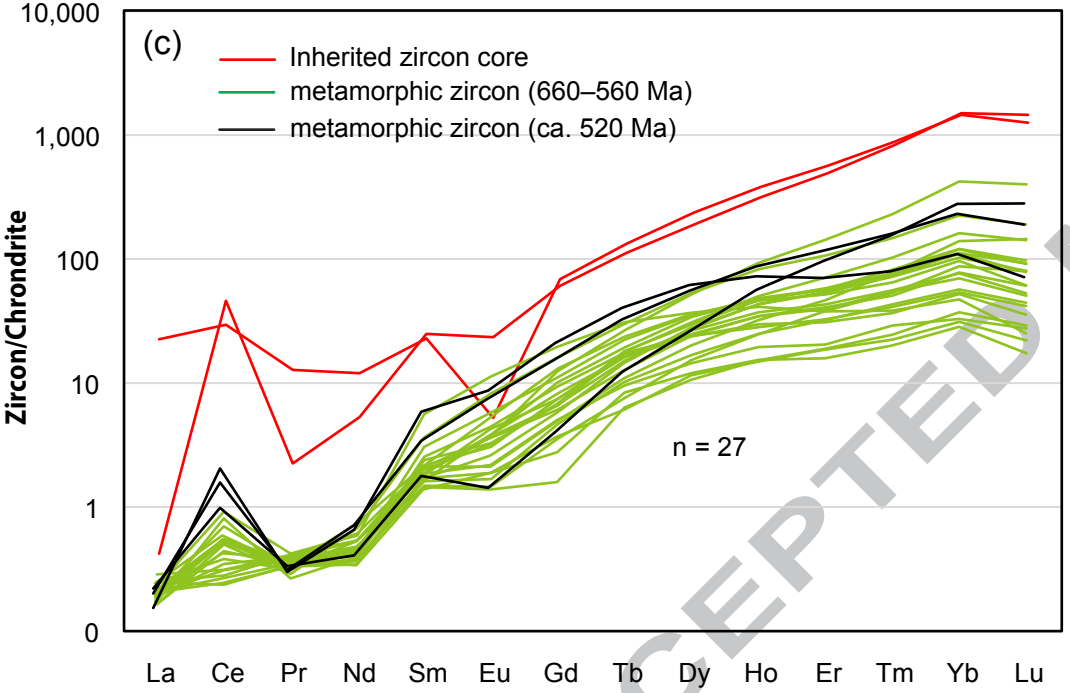


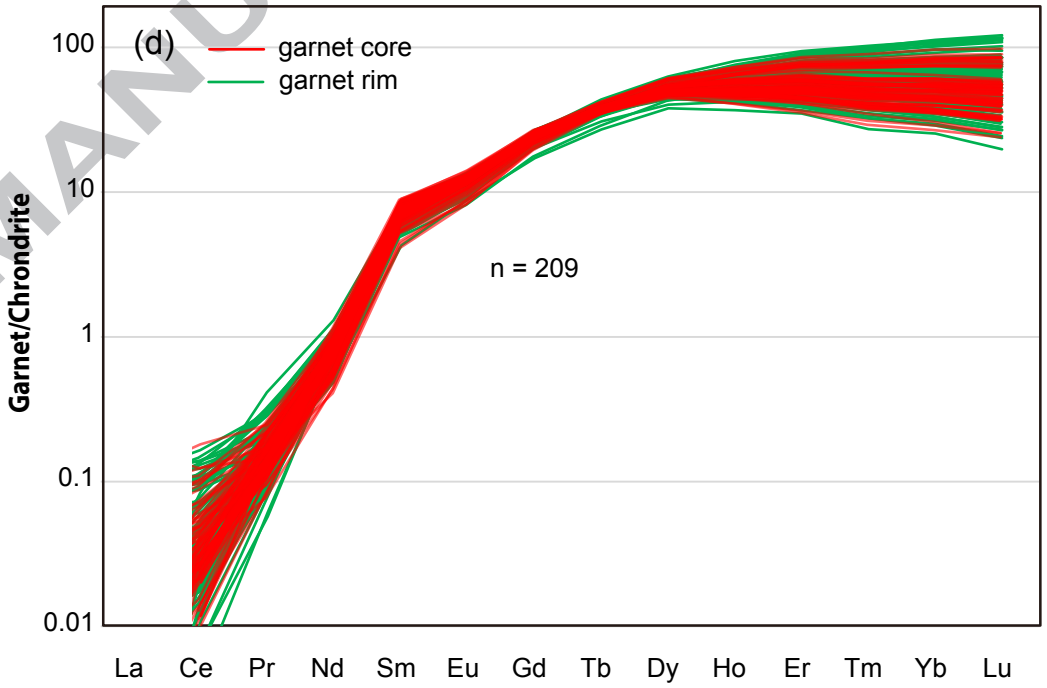


ACCEPTED MANUSCRIPT



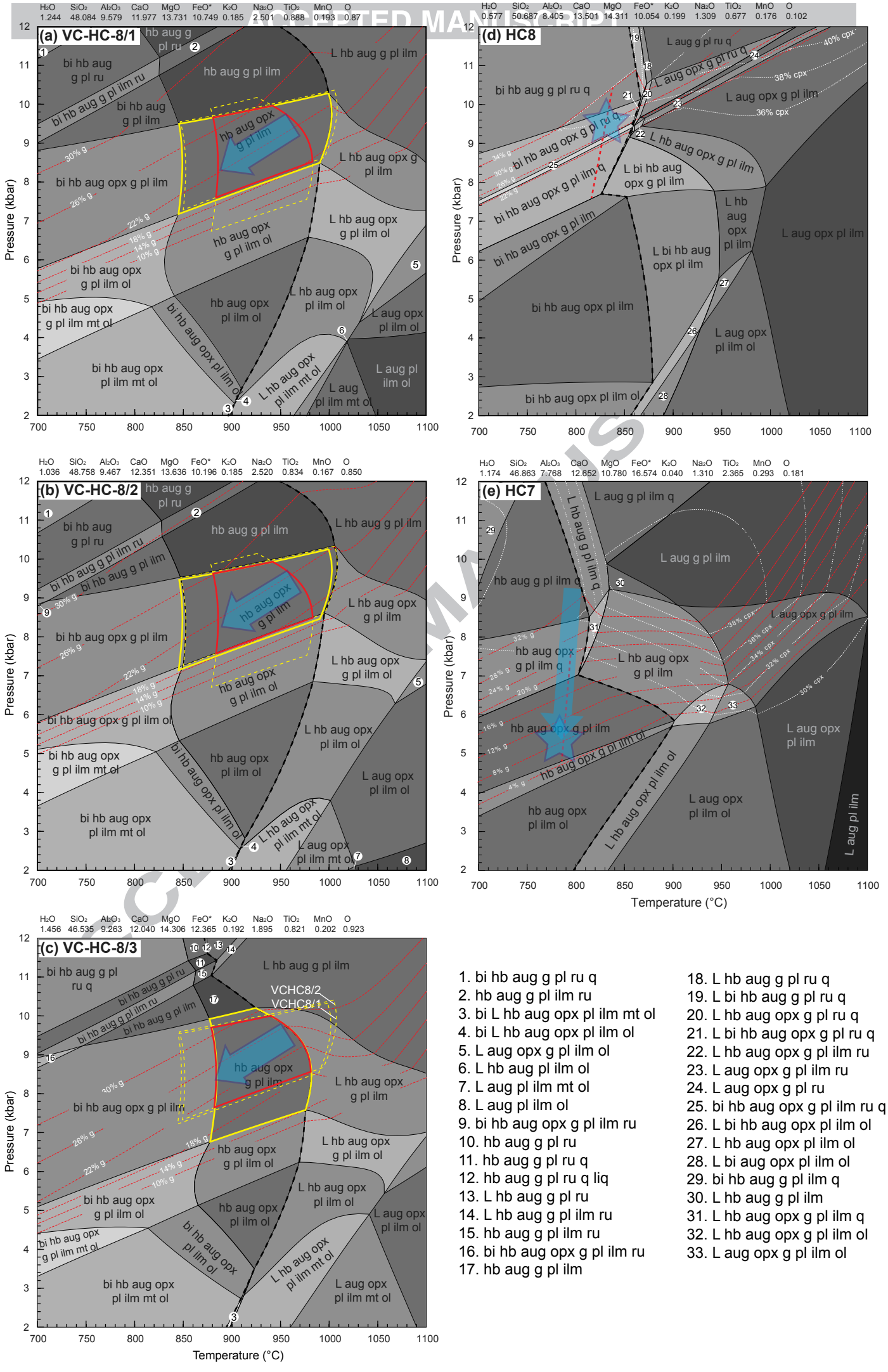






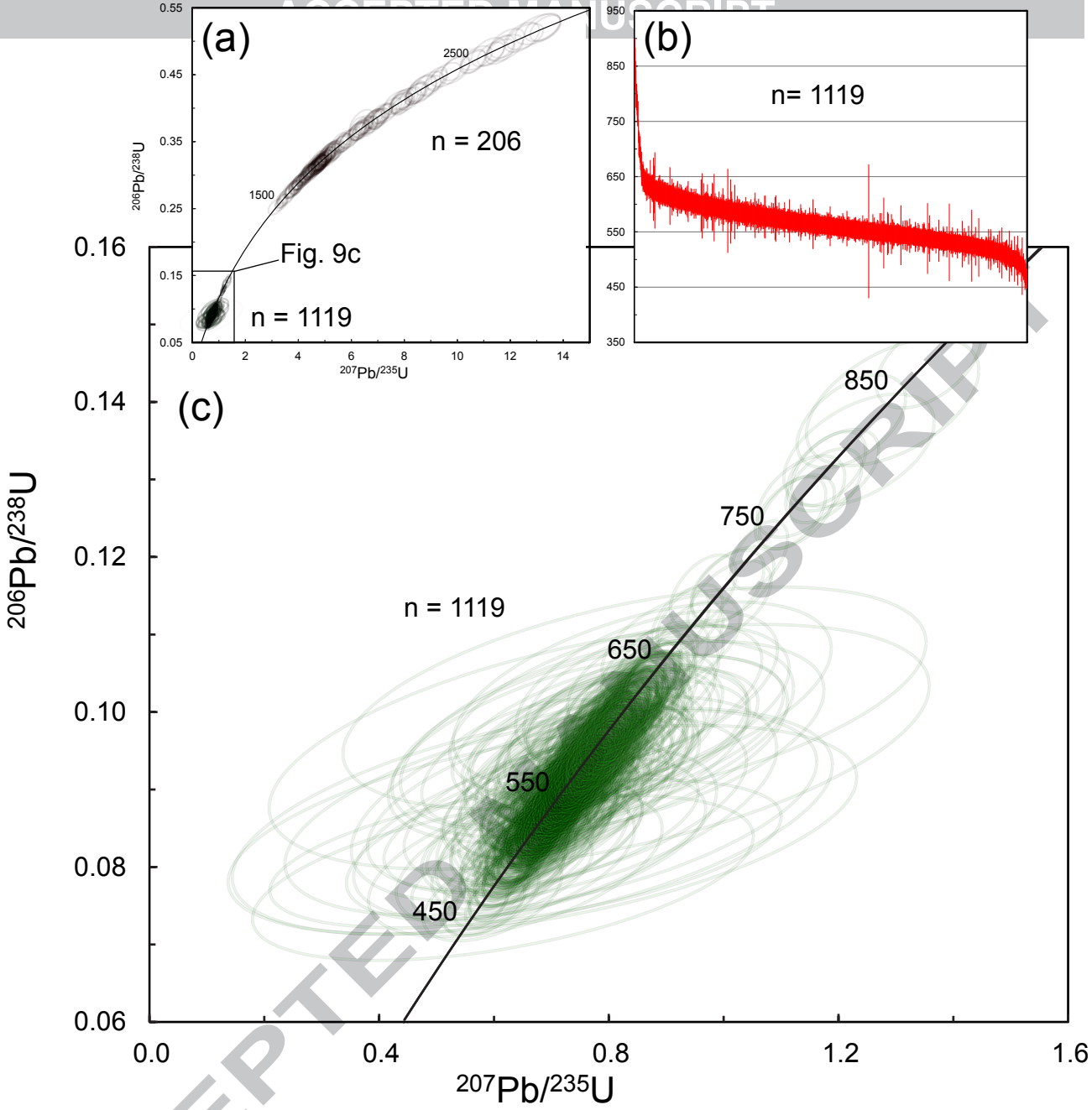
ACCEPTED MANUSCRIPT

ACCEPTED MANUSCRIPT



1. bi hb aug g pl ru q
2. hb aug g pl ilm ru
3. bi L hb aug opx pl ilm mt ol
4. bi L hb aug opx pl ilm ol
5. L aug opx g pl ilm ol
6. L hb aug pl ilm ol
7. L aug pl ilm mt ol
8. L aug pl ilm ol
9. bi hb aug opx g pl ilm ru
10. hb aug g pl ru
11. hb aug g pl ru q
12. hb aug g pl ru q liq
13. L hb aug g pl ru
14. L hb aug g pl ilm ru
15. hb aug g pl ilm ru
16. bi hb aug opx g pl ilm ru
17. hb aug g pl ilm
18. L hb aug g pl ru q
19. L bi hb aug g pl ru q
20. L hb aug opx g pl ru q
21. L bi hb aug opx g pl ru q
22. L hb aug opx g pl ilm ru
23. L aug opx g pl ilm ru
24. L aug opx g pl ru
25. bi hb aug opx g pl ilm ru q
26. L bi hb aug opx pl ilm ol
27. L hb aug opx pl ilm ol
28. L bi aug opx pl ilm ol
29. bi hb aug g pl ilm q
30. L hb aug g pl ilm
31. L hb aug opx g pl ilm q
32. L hb aug opx g pl ilm ol
33. L aug opx g pl ilm ol

ACCEPTED MANUSCRIPT



ACCEPTED MANUSCRIPT